MATHEMATISCHES FORSCHUNGSINSTITUT OBERWOLFACH

Report No. 3/2007

Trends in Mathematical Imaging and Surface Processing

Organised by
Caselles, Vicent (Barcelona)
Dziuk, Gerhard (Freiburg)
Rumpf, Martin (Bonn)
Schröder, Peter (Pasadena)

January 21st – January 27th, 2007

ABSTRACT. Motivated both by industrial applications and the challenge of new problems, one observes an increasing interest in the field of image and surface processing over the last years. It has become clear that even though the applications areas differ significantly the methodological overlap is enormous. Even if contributions to the field come from almost any discipline in mathematics, a major role is played by partial differential equations and in particular by geometric and variational modeling. The aim of the workshop was to gather a group of leading experts coming from mathematics, engineering and computer graphics to cover the main developments.

Introduction by the Organisers

In the area of image and surface processing a real interplay between engineers, computer scientists and mathematicians has been occuring over the last decade. Even though the application areas differ significantly, the methodological overlap is enormous. Contributions to the field come from almost any discipline of mathematics. A major role is played by partial differential equations and in particular by geometric and variational modeling. We see increasing numbers of examples of work in imaging and computer graphics which significantly improve the state of the art techniques developed in traditional disciplines and in particular inspire novel work in mathematics. Some of the many examples discussed during the workshop include the global minimization of new functionals based on methods from discrete optimization theory, the modeling and treatment of manifold topology based

on projections, or subtle subdivision techniques to ensure curvature continuity in surface modeling.

The intention of this workshop was to further stimulate the exchange of new methodology and ideas. The workshop brought together mathematicians working on the calculus of variations, on differential and discrete geometry, on partial differential equations, and on numerical analysis with leading experts in computer graphics, image processing and computer vision. In addition about ten junior researchers joined the workshop in a lively interplay with more senior participants.

The role of geometry, analysis and numerical analysis for PDE-based image and surface models is of central importance. Many of the models involve minimizing geometric functionals of first (area) or second order (Willmore-functional). The role of analysis is to predict the qualitative behaviour of solutions of the resulting highly nonlinear partial differential equations. Lectures on thresholding approaches, level set methods and max flow - min cut algorithms were dealing with this topic. Numerical analysis plays a decisive role in the derivation and construction of efficient and robust algorithms. For instance, efficient numerical schemes for the restoration of destroyed or missing areas in images and the error control for discretization of total variation functionals in imaging were addressed in lectures during the workshop. A particular focus was on the solution of geometric partial differential equations and the minimization of geometric functionals and their discretization, which leads directly into extremely difficult analytic problems and questions of convergence of the corresponding discrete schemes. Extensive discussions occurred regargind the question of conversion of analytical and geometric insights into fast and effective algorithms for challenging applications such as the design of glass roofs, the extraction of motion fields from image sequences, the similarity analysis of shapes or the topological persistent fairing of surfaces from 3D scanning devices, and many others.

Aside from 20 main lectures, junior participants presented their own work in a special two hour session through a series of short presentations:

Leah Bar (Minneapolis)
Restoration of Images with Piecewise Space-Variant Blur
Benjamin Berkels (Bonn)
Identification of grain boundary contours at atomic scale
Juan Cardelino (Barcelona)
Region based segmentation using the tree of Shapes
Milena Chermisi (Roma)
Level Set Method for systems of PDEs
Marc Droske (Berlin)
Higher-Order Feature-Preserving Regularization of Curves and Surfaces
Carsten Eilks (Freiburg)
The Cahn-Hilliard equation on moving parametric surfaces

Matthew Elsey (Ann Arbor)
Fairing of Triangulated Surfaces Using Total Absolute Gaussian Curvature
Michael Fried (Erlangen)
Iterative Level Set Based Segmentation in Remote Sensing
Markus Grasmair (Innsbruck)
The taut string algorithm for total variation regularization
Lin He (Linz)
Solving the Chan-Vese Model by a Multiphase Level Set Algorithm Based on the Topological Derivative
Claus Heine (Freiburg)
Finite Elements on Unfitted Meshes
Luca Lussardi (Palaiseau)
Free discontinuity functionals with linear growth and their approximation
Bernhard Mößner (Freiburg)
Solving the Stokes-equations with B-Splines
Paola Pozzi (Freiburg)
Anisotropic Mean Curvature Flow in Higher Codimension

Workshop: Trends in Mathematical Imaging and Surface Processing

Table of Contents

Abstracts

Fair triangulated surfaces from positional constraints at interactive rates

Marc Alexa

(joint work with Takeo Igarashi, Andrew Nealen, Olga Sorkine)

Several computer applications require the computation and manipulation of a fair triangulated surface in fractions of a second. We achieve this interactive response time for moderately sized meshes by modeling a non-linear problem as the iterative solution of several linear systems with constant system matrices. These matrices are factored in a pre-process and during interaction only few back-substitutions are necessary.

Let the triangulation be defined by the edge graph $\{(i,j)\} = E$ and its embedding by vertex positions $\mathbf{v}_i \in \mathbf{V}$. We assume E is constant and want to derive vertex positions $\mathbf{V}$ so that few constrained vertices are close to given locations $\mathbf{v}_i', i \in C$ from a subset of vertices C, i.e. $\mathbf{v}_i \approx \mathbf{v}_i'$, and the embedded geometry is an (approximate) solution to the PDE $\Delta_B H = 0$, where Δ_B is the (discrete) Laplace-Beltrami operator, and $H = (\kappa_1 + \kappa_2)/2$ is the mean curvature.

The graph Laplacian

$$(1) \qquad\qquad\qquad \mathbf{L} = \mathbf{D} - \mathbf{A}$$

with $\mathbf{D} = \mathrm{diag}(d_i), d_i = \#\{(i,j) \in E\}$ the matrix of vertex degrees and the adjacency matrix $\mathbf{A} = \{a_{ij}\}, a_{ij} = \#\{(i,j) \in E\}$, is independent of the embedding of the triangulation and fails to account for the metric of the surface. Taking the metric of the surface into account leads to a similarly structured but differently weighted Laplacian operator L_c, where the weights depend on cotangents of interior angles in the star of a vertex [1]. In contrast to the smooth case, $L_c \mathbf{v}$ is the integrated mean curvature around $\mathbf{v}$ and the pointwise scalar mean curvature in vertex i is given as $H_i \mathbf{n}_i = m_i^{-1} L_c \mathbf{v}_i$ where $\mathbf{n}_i$ is the unit normal and m_i is the measure assigned to the vertex [6] (e.g. the area of Voronoi cell in the embedded triangulation).

We factor the PDE into two second order problems and solve them repeatedly [3]. In the first step target mean curvatures $\mathbf{H} = \{H_i\}$ are smoothed (i.e. $L_c \mathbf{H} = 0$ plus boundary constraints). Then, disregarding positional constraints, solving $L_c \mathbf{V} = \mathbf{N}$, where $N = \{a_i H_i \mathbf{n}_i\}$, moves vertices into positions that satisfy the curvature constraints. However, as L_c depends on the embedding, each iteration requires solving a new linear system, which we have found to be too slow in practice.

Note that $L = L_c$ (up to a constant) if all edges have equal length (i.e. there is no metric distortion). The main idea of our approach is, therefore, to generate edges of approximately equal length in the triangulation. Starting from an arbitrary general position of the vertices (i.e. at least a subset of the vertices admit the

computation of curvatures and not all edge lengths are zero) we compute target mean curvatures by solving

$$(2) \qquad \arg\min_c \left\{ \sum_i \|\mathbf{L}(H_i)\|^2 + \sum_i \|H_i - H_i'\|^2 \right\},$$

where H_i' is the scalar mean curvature at vertex i (if available); and similarly

$$(3) \qquad \arg\min_e \left\{ \sum_i \|\mathbf{L}(e_i)\|^2 + \sum_i \|e_i - e_i'\|^2 \right\},$$

for a smooth set $\{e_i\}$ of target average edge lengths per vertex, from the current set of the average lengths e_i' of edges incident on vertex i. Note that the least squares formulations above are an approximation to the projection onto low frequency eigenvectors of L [4]. From these target scalar values we compute target mean curvature vectors

$$(4) \qquad \delta_i = m_i \cdot H_i \cdot \mathbf{n}_i$$

and target edge vectors

$$(5) \qquad \eta_{ij} = (e_i + e_j)/2 \cdot (\mathbf{v}_i - \mathbf{v}_j)/\|\mathbf{v}_i - \mathbf{v}_j\|.$$

based on the current embedding (i.e. area measures m_i and vertex normals $\mathbf{n}_i$ are computed from the current triangles). The vertex positions are updated by solving

$$(6) \qquad \arg\min_{\mathbf{V}} \left\{ \sum_i \|\mathbf{L}(\mathbf{v}_i) - \delta_i\|^2 + \sum_{(i,j) \in B} \|\mathbf{v}_i - \mathbf{v}_j - \eta_{ij}\|^2 + \sum_{i \in C} \|\mathbf{v}_i - \mathbf{v}_i'\|^2 \right\}.$$

We have found that it is sufficient to only constrain a subset of edges B, i.e. the edges incident to the constrained vertices, because setting the uniformly discretized Laplacian equal to vectors in normal direction automatically improves inner fairness at all unconstrained vertices [2].

We have implemented this procedure by factorizing the sparse matrices in a pre-process [5], and then at run-time repeatedly updating target curvatures, edge lengths, and positions by back-substitution. We observed that the computation converges rather quickly, in approximately 5 to 10 iterations, which requires fractions of a second for triangulations of a several hundred vertices.

References

[1] M. Meyer, M. Desbrun, P. Schröder, and A. H. Barr. Discrete differential-geometry operators for triangulated 2-manifolds. In H.-C. Hege and K. Polthier, editors, *Visualization and Mathematics III*, pages 35–57. Springer-Verlag, Heidelberg, 2003.

[2] Nealen, A., Sorkine, O., Alexa, M., and Cohen-Or, D. A sketch-based interface for detail-preserving mesh editing. *ACM Trans. Graph. 24*, 3, 1142–1147, 2005

[3] Schneider, R., and Kobbelt, L. Geometric fairing of irregular meshes for free-form surface design. *Computer Aided Geometric Design 18*, 4, 359–379, 2001

[4] O. Sorkine and A. Nealen A note on Laplacian mesh smoothing. *submitted.*

[5] Toledo, S. Taucs: *A Library of Sparse Linear Solvers.* Tel Aviv University, 2003

[6] WARDETZKY, M., BERGOU, M., HARMON, D., ZORIN, D., AND GRINSPUN, E. Discrete quadratic curvature energies. *CAGD (to appear)*, 2007

Topological and variational properties of a model for reconstructing three-dimensional images

GIOVANNI BELLETTINI

(joint work with V. Beorchia and M. Paolini)

We have discussed a two-dimensional variational model for the reconstruction of a smooth generic three-dimensional transparent scene E. Here the symbol E denotes a solid set in $(-1, 1) \times \Omega$ with a finite number of disjoint smooth connected components, where Ω is an open domain of $I\!\!R^2$ representing the screen. The model may handle self-occlusions and could be considered as an improvement of the 2.1D sketch proposed by Nitzberg and Mumford [6], see also [7] and [2]. Roughly, E is generic if its *apparent contour* G_E in the direction e_1 of the observer has singularities which are stable under small perturbations of ∂E [9]. The planar graph G_E is defined as the orthogonal projection on Ω of the critical curve

$$M_E := \{z \in \partial E : \text{ the tangent plane to } \partial E \text{ at } z \text{ contains } I\!\!R e_1\}.$$

In order to introduce the variational model one needs an analysis of the apparent contour of E. Hence, using the so-called Huffman labelling [3], we preliminarly characterize those planar graphs that are apparent contours of some three-dimensional generic scene. See also [10] and [4] for a description of this result and for other applications, and [8], [5] for related problems. The labelling is based on two functions. The first one is the function $f_E : \Omega \to 2\mathbb{N}$, which jumps of two units exactly on G_E, and counts the total number of layers of ∂E in front of a point x in the screen Ω. The second function $d_E : G_E \to \mathbb{N}$ counts the number of layers of ∂E in front of the point $z \in M_E$ corresponding to the point $x \in G_E$, x not a singular point of G_E. The labelling then requires a number of compatibility conditions between f_E and d_E.

Beside the above mentioned existence result, we also show that if E and F are two three-dimensional scenes having the same apparent contour, then E and F must differ by a homeomorphism of $(-1, 1) \times \Omega$, strictly increasing on each fiber along e_1.

We are now in the position of identifying the domain of the functional $\mathcal{F}$ describing the model: $\mathrm{Dom}(\mathcal{F})$ consists of the triplets (f, d, u), where f and d have the qualitative properties described above, and u (the function supposed to reconstruct the given gray level $g \in L^\infty(\Omega)$) is smooth out of the *visible* part $\{d = 0\}$ of the jump J_f of f. The functional $\mathcal{F}$ takes essentially the form

$$\mathcal{F}(f, d, u) := \#(\mathrm{ver}(J_f)) + \int_{J_f \setminus \mathrm{ver}(J_f)} (1 + \mathrm{vert}\kappa\mathrm{vert}^p) \, ds$$

$$+ \int_{\Omega \setminus \{d=0\}} \mathrm{vert}\nabla u\mathrm{vert}^2 \, dx + \int_{\Omega} \mathrm{vert}u - g\mathrm{vert}^2 \, dx,$$

where $\#$ counts the set $\mathrm{ver}(J_f)$ of the singular points of J_f, κ is the curvature of J_f, $p \in (1,2)$, and f and d must satisfy all compatibility conditions devised by the previous topological analysis. The exponent $p = 2$ is not allowed, since the curvature of the canonical cusp is not square-integrable. Note that u is smooth along the invisible contour $\{d > 0\}$ of J_f. Finally, given g, in order to reconstruct a corresponding reasonable three-dimensional scene, first we minimize $\mathcal{F}$ among all admissible triplets and produce one minimizing triplet. Then we find the corresponding generic scene using the topological theorems.

Note that identifying the domain of the relaxed functional $\overline{\mathcal{F}}$ of $\mathcal{F}$ could be useful toward understanding whether a given finite union of arcs is contained in the visible part of the apparent contour of some three-dimensional scene.

We conclude by mentioning that the problem of classifying three-dimensional isotopic surfaces via a complete set of elementary moves on the corresponding apparent contours can be handled with a computer program, and is under investigation.

The above results have been obtained in collaboration with Valentina Beorchia (Univ. Trieste, Italy) and Maurizio Paolini (Università Cattolica Brescia, Italy), see [1].

REFERENCES

[1] G. Bellettini, V. Beorchia and M. Paolini, *Topological and variational properties of a model for the reconstruction of three-dimensional transparent images with self-occlusions*, Preprint Centro De Giorgi, 2006, submitted. Available at http://www.cvgmt.sns.it.

[2] G. Bellettini and M. Paolini, *Variational properties of an image segmentation functional depending on contours curvature*, Adv. Math. Sci. Appl., **5** (1995), pp. 681–715.

[3] D.A. Huffman, *Impossible objects as nonsense sentences*, in Machine Intelligence 6, B. Meltzer and D. Michie Eds., American Elsevier Publishing Co., New York 1971.

[4] O.A. Karpenko and J.F. Hughes, *SmoothSketch: 3D free-form shapes from complex sketches*, Preprint 2006, to appear on Siggraph'06.

[5] D. Luminati, *Surfaces with assigned apparent contour*, Ann. Sc. Norm. Super. Pisa, Cl. Sci., IV. Ser. 21, **3** (1994), 311-341.

[6] M. Nitzberg and D. Mumford, *The 2.1-D sketch*, Proceedings of the Third International Conference on Computer Vision, Osaka, 1990.

[7] M. Nitzberg, D. Mumford and T. Shiota, *Filtering, Segmentation and Depth*, Vol. 662 of Lecture Notes in Computer Science 662, Springer-Verlag, Berlin, 1993.

[8] R. Pignoni, *On surfaces and their contour*, Manuscripta Math., **72** (1991), 223-249.

[9] H. Whitney, *On singularities of mappings of euclidean spaces. I. Mappings of the plane into the plane*, Ann. of Math., **62** (1955), 374-410.

[10] L.R. Williams, *Topological reconstruction of a smooth manifold-solid from its occluding contour*, Int. J. Computer Vision, **23** (1997), 93–108.

Movie Denoising by Average of Warped Lines

Marcelo Bertalmío

(joint work with Vicent Caselles, Álvaro Pardo)

Image denoising is one of the most studied problems in the image processing community. Within the area of image sequence denoising we can distinguish different cases regarding the source material, the specific type of noise and its application. In our case the motivation to study this problem is the restoration of old films. Nevertheless, the ideas here presented can be adapted to other types of image sequences: biological (3D), ultrasound, infrared, compressed (with coding noise), etc.

Before going into details of image sequence denoising we are going to discuss three key issues. First, it is important to consider the different types of noise that can be present in the image sequence. Noise in image sequences can be produced during acquisition by the sensor, due to errors during its transmission, by coding noise, etc. Therefore, the current research is addressed to develop methods that can deal with different types of noise.

The second issue is the degradation of the original content of the sequence: we must respect as much as possible the original content of the sequence (details, texture, motion, etc) without introducing artifacts during the denoising process. In addition to the unpleasant visual distortions that can affect the original content, the degradation of the original content may also affect further processing steps as: segmentation, motion estimation, compression, etc.

Finally, the last issue is the computational complexity of the method and its number of parameters. Due to the enormous amount of data present in image sequences the proposed schemes must be automatic, without a large number of parameters, and computationally lightweight. Although it is not necessary to have a real time method, the method must provide results in a reasonable time in order to allow an interactive process with the user.

Although we can apply existing static image denoising methods to the case of image sequences[1] (intra-frame methods), we can do better by including temporal information (inter-frame methods) (see [1]). This temporal information is crucial since our perception is very sensitive to temporal distortions like edge displacement: the disregard of temporal information may lead to temporal inconsistencies in the result. Filters which take into account the 3D image support can be classified into motion adaptive filters and motion compensated filters [1]. Motion adaptive filters take into account the dynamic character of the sequence but do not compute the optical flow. They are based on averaging pixels of different frames trying to avoid the blurring effect where motion occurs, they are the temporal counterpart of edge preserving spatial filters in that temporal edges are related to motion. Examples include different types of adaptive median filters and order statistic filters [2, 3] or recursive filters [4, 5] (see [1]). Motion compensated filters

---

[1]For now on, we will concentrate in temporal sequences leaving out 3D images. However, several of the comments and ideas here presented can be applied to the latter case.

are based on the assumption that the variation of the pixel gray level over a motion trajectory is mainly due to noise and, thus, averaging these values should give a good estimate of the true pixel value; they produce high quality results. The motion compensated spatio-temporal LMMSE was proposed by [6] and studied in [7] (these filters are an extension of spatial LMMSE filters introduced in [8, 9]). A related method which implicitly compensates for motion by performing 1-D signal estimation along a set of hypothesized motion directions was proposed in [10]. In [11] the authors introduced an Adaptive Weighted Algorithm (AWA) which can be interpreted as a motion compensated neighborhood filter. We refer to [1] for a more detailed account of these methods.

Unfortunately, motion estimation is an ill-posed problem (that needs extra conditions in order to be solved) and its estimation is not straight forward in the case of noisy sequences. To overcome the problem of motion estimation, Buades et. al., based on their previous work [12], presented a method (the NLM method) for image sequence denoising that does not need motion estimation [13]. Starting from the idea that averaging several independent realizations of the same random variable reduces noise, they present a method for image denoising that considers a weighted average of similar samples. Similar samples (pixels) are found comparing their neighborhoods: two pixels with similar neighborhoods are said to be similar. This approach can be rooted to the pioneering work of Efros-Leung [14]. The main feature of these methods is that they may look for similar neighborhoods all over the image (or sequence)[2]. In this way they find many similar samples for the denoising procedure. For a detailed review of neighboring filters and PDE-based methods we refer the reader to [12]. In [15] the authors extend their work on Field of Experts [16] in order to deal with grain noise in archival film. They develop a model of grain noise that is used as a prior in the Field of Experts framework.

The main purpose of this talk is to propose an efficient method for denoising digital image sequences without using motion estimation. The main idea behind our proposal is similar to the one used in [13] and [17]. For each pixel we look for a set of similar samples to be used in the filtering step: we estimate the nearby points on the level surface passing trough it, we consider them as realizations of the same random variable and we take an average of them. For that purpose, we present an efficient method to find similar samples via warping lines in spatio-temporal neighborhoods. Our main concerns are: the computational cost of our algorithm, its unsupervised nature, its capabilities to automatically deal with different kinds of noise (even if the method is based on the assumption of additive white noise) and its possibilities to respect the visual details on the image sequence. As we will see, the proposed method obtains good denoising results with smaller computational complexity than the methods proposed in [13, 17].

<div align="center">REFERENCES</div>

[1] A. Tekalp, *Digital Video Processing*. Prentice Hall, 1995

---

[2]As we will see later, this is usually unpractical and similar samples are found in the proximity of the pixel to be processed.

[2] B. Alp, P. Haavisto, T. Jarske, K. Oistamo, and Y. Neuvo, *Median based algorithms for image sequence processing*, Proceedings SPIE Visual Comm. and Image Proc. '90, 1990, pp.122-134.

[3] G. Arce, *Multistage order statistic filters for image sequence processing*, IEEE Transactions Signal Processing, vol. 39, pp. 1146-1163, 1991.

[4] E. Dubois and S. Sabri, *Noise reduction in image sequences using motion compensated temporal filtering*, IEEE Transactions on Communications, vol. 32, no. 7, pp.826-832, July 1984.

[5] R.H. McMann, S. Kreinik, J.K. Moore, A. Kaiser, and J. Rossi, *A digital noise reducer for encoded NTSC signals*, SMPTE Journal, vol. 87, pp. 129-133, March 1979.

[6] R. Samy, *An adaptive image sequence filtering scheme based on motion detection*, SPIE, 1985, pp. 135-144.

[7] M. Sezan, M. Ozkan and S. Fogel, *Temporally adaptive filtering of noisy image sequences using a robust motion estimation algorithm*, Proc. IEEE Int. Conf. Acoust. Speech, Signal Processing, 1991, pp.2429-2432.

[8] J. Lee, *Digital image smoothing and the sigma filter*, Computer Vision, Graphics and Image Processing, vol. 24, pp. 255-269, 1983.

[9] D. Kuan, A. Sawchuk, T. Strand and P. Chavel, *Adaptive noise smoothing filter for images with signal-dependent noise*, IEEE Transcations Pattern Anal. Mach. Intell., vol. 7, pp. 165-177, March 1985.

[10] D. Martinez and J. S. Lim, *Implicit motion compensated noise reduction of motion video scenes*, Proc. Acoustics, Speech, and Signal Processing (ICASSP'85), 1985, pp. 375-378.

[11] M.K.Ozkan, M. Sezan and A. Tekalp, *Adaptive motion compensated filtering for noisy image sequences*, IEEE Transcations Circuits and Systems for Viedeo Technology, vol. 3, pp. 277-290, August 1993.

[12] A. Buades, B. Coll and J.M. Morel, *A review of image denoising algorithms, with a new one*, SIAM Multiscale Modeling and Simulation, vol. 4, no. 2, pp. 490-530, 2005.

[13] A. Buades, B. Coll, J.M. Morel, *Denoising image sequences does not require motion estimation*, Proc. IEEE Conf. on Advanced Video and Signal Based Surveillance, 2005, pp. 70-74.

[14] A. Efros and T. Leung, *Texture synthesis by non-parametric sampling*, IEEE Int. Conf. on Computer Vision, ICCV'99, 199, pp. 1033-1038.

[15] T. M. Moldovan, S. Roth and M. J. Black, *Denoised archival films using a learned bayesian model*, ICIP2006, 2006.

[16] S. Roth and M. J. Black, *Fields of Experts: A framework for learning image priors*, IEEE Conf. on Computer Vision and Pattern Recognition, vol. 2, June 2005, pp. 860-867.

[17] J. Boulanger and C. Kervrann and P. Bouthemy, *Adaptive space-time patch-based method for image sequence restoration*, Workshop on Statistical Methods in Multi-Image and Video Processing (SMVP'06), May 2006.

Fast Image Inpainting

FOLKMAR BORNEMANN

(joint work with Tom März)

Nontexture *image inpainting* is the task of restoring a digital image $u_h^0 : \Omega_h \setminus D_h \to [0,1]$ for a destroyed, or consciously marked, subregion D_h of the image domain Ω_h by continuing the geometric information given by the isophotes. The result is a restored image $u_h : \Omega_h \to [0,1]$. (In reminiscence of a discretization, pixelized domains and quantities will be denoted by a subscript h. Quantization of gray levels will be neglected.)

Techniques of nonlinear partial differential equations have successfully been applied to this problem. The equations and algorithms are essentially based on one of the following paradigms:

- variational models (starting with the seminal work [3])
- phenomenological models (starting with the seminal work [1])

However, the resulting algorithms are based on *iteration*, mostly in the form of a (pseudo-) time embedding, or on dynamical programming and do not have, so far, a complexity that is optimal in the number of pixels to be inpainted.

Our work [2] shows that pdes can enter the problem in yet another fashion: By analyzing a discrete algorithm in the limit of infinite spatial resolution. This analysis allows to understand and correct the defects of the algorithm. Starting with a non-iterative method due to Telea [4], which has optimal complexity, we succeeded in keeping the optimal complexity while improving dramatically upon the quality of the method.

(a) geometric setting of the discrete algorithm   (b) geometric setting of the high-resolution limit
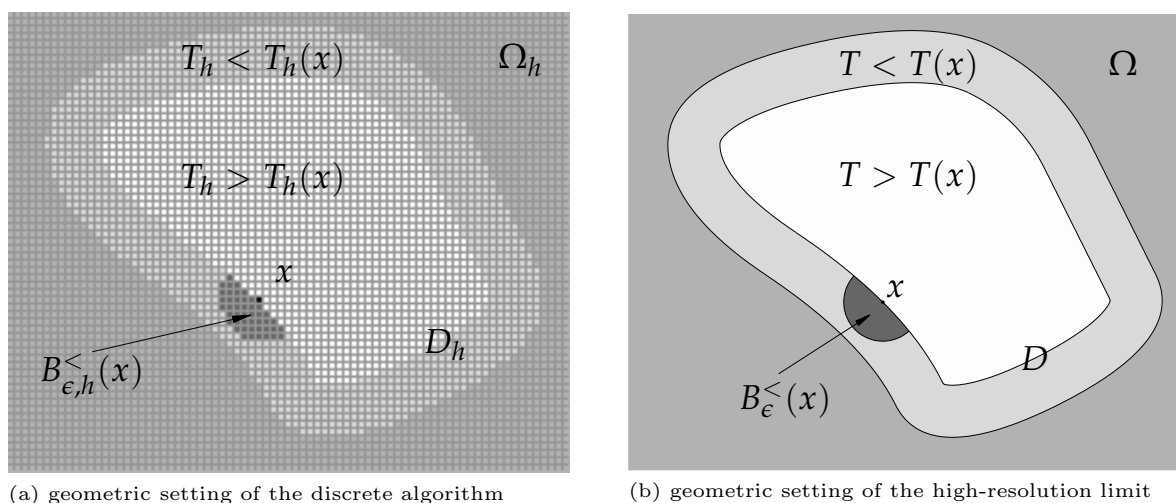
FIGURE 1. The geometric idea of the inpainting algorithm.

Telea's method orders the pixels of the inpainting domain D_h by increasing distance $T_h(x)$ to the boundary ∂D_h ("onion peel", see Fig. 1),

$$D_h = \{x_1, \ldots, x_N\}$$

and takes weights over neighborhoods $B_{\epsilon,h}^<(x_k) = B_{\epsilon,h} \setminus \{x_k, \ldots, x_N\}$ of already inpainted pixels:

$$u_h|_{\Omega_h \setminus D_h} = u_h^0,$$

$$u_h(x_k) = \frac{\displaystyle\sum_{y \in B_{\epsilon,h}^<(x_k)} w_h(x_k, y)\, u_h(y)}{\displaystyle\sum_{y \in B_{\epsilon,h}^<(x_k)} w_h(x_k, y)}, \qquad k = 1, \ldots, N.$$

Telea suggests to use the weight function

$$w_h(x,y) = \frac{|\nabla_h T_h(x) \cdot (x-y)|}{\|x-y\|^2}.$$

We can prove that in the high resolution ($h \to 0$) and vanishing viscosity ($\epsilon \to 0$) limit, Telea's algorithm results in the hyperbolic boundary value problem

$$\vec{n}(x) \cdot \nabla u(x) = 0 \quad \text{on } D \setminus \Sigma, \qquad u|_{\partial D} = u^0|_{\partial D},$$

where $\vec{n}(x) = \nabla T(x)$ denotes the vector field normal to the level lines of the distance map $T(x)$ to the boundary ∂D. Further, Σ denotes the Euclidean skeleton of the inpainting domain D, that is, the locus where the characteristics of $\vec{n}$ intersect the first time. This limit equation perfectly explains the behavior of the algorithm as shown in Fig. 2(b).

(a) inpainting domain: 228×108 px^2 (b) Telea's method, $\epsilon = 6$ px   (c) our method, $\mu = 100$, $\epsilon = 6$ px

FIGURE 2. The skeleton: $\Sigma \setminus \Sigma_{\text{trans}}$ red, Σ_{trans} green, ∂D blue.
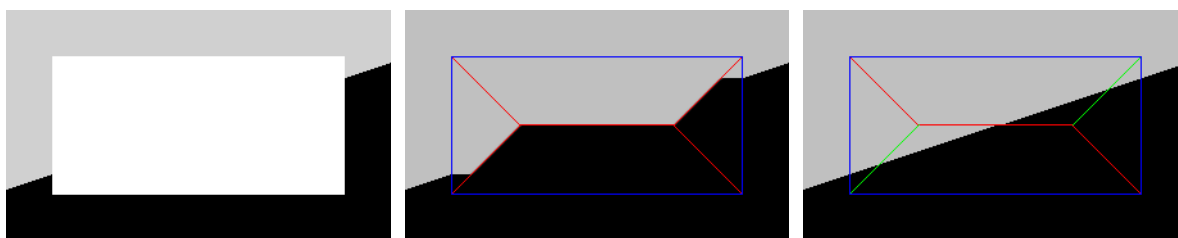
If, instead, for a given normalized vector field $\vec{c}(x)$, we take the weight function

$$w(x,y) = \sqrt{\frac{\pi}{2}} \frac{\mu}{\|x-y\|} \exp\left(-\frac{\mu^2}{2\epsilon^2} \left|\vec{c}^{\perp}(x) \cdot (x-y)\right|^2\right),$$

we get the limit boundary value problem

$$\vec{c}_*(x) \cdot \nabla u(x) = 0 \quad \text{on } D \setminus \Sigma, \qquad u|_{\partial D} = u^0|_{\partial D}.$$

Here, $c_*(x)$ is a normalized, *effective* vector field that satisfies

$$\lim_{\mu \to \infty} \vec{c}_*(x) = \begin{cases} \vec{c}(x), & \vec{n}(x) \cdot \vec{c}(x) > 0, \\ -\vec{c}(x), & \vec{n}(x) \cdot \vec{c}(x) < 0, \\ \vec{n}(x), & \vec{n}(x) \perp \vec{c}(x). \end{cases}$$

Thus, except for the singular case of *tangency* (with respect to the level lines of the distance map), the effective vector field $\vec{c}_*(x)$ aligns itself parallel to the given vector field $\vec{c}(x)$. For a correctly chosen $\vec{c}(x)$, the improvement resulting in the algorithm is clearly visible in Fig. 2(c).

The necessity of the exceptional case can be understood from an analysis of the well-posedness of the limit boundary value problem. Moreover, this analysis shows that there is a certain part Σ_{trans} of the skeleton, which we call the *transparent* part, that unconditionally allows for the continuation of geometric information.

Only at the remaining nontransparent parts of the skeleton there is the possibility of jumps in the gray level for badly chosen vector fields $\vec{c}(x)$.

We suggest to choose $\vec{c}(x)$ as the *coherence* direction, that is, the vector field that gives

$$\vec{c}(x) \cdot \nabla u(y) \approx 0, \qquad y \in B_\rho^<(x),$$

in the sense of least squares. For a real color image, Fig. 3 illustrates the behavior of the resulting algorithm in comparison to Telea's method.

(a) destroyed image $(241 \times 159\text{px}^2)$ (b) Telea's method $(0.08\,\text{sec})$ (c) our method $(0.4\,\text{sec})$

FIGURE 3. Image inpainting: Telea's vs. our method.

Open Problem. In fact, there are two choices in Telea's algorithm that can be made without changing its complexity: The weight function $w(x, y)$, which we actually have changed, and the order by distance, which we have not changed so far. We conjecture that by changing the order we will be able to address the singular case of tangency. First experiments indicate that a modified distance function $T(x)$ subject to a generalized Eikonal equation $F(x)\|\nabla T(x)\| = 1$, $T|_{\partial D} = 0$, might do the job.

REFERENCES

[1] Bertalmio, M., Sapiro, G., Caselles, V. and Ballester, C.: Image inpainting, *SIGGRAPH '00: Proc. 27th Conf. on Computer Graphics and Interactive Techniques, New Orleans*, ACM Press/Addison-Wesley, New York (2000), pp. 417–424.
[2] Bornemann, F. and März, T.: Fast Image Inpainting Based on Coherence Transport, submitted to JMIV (2006), `http://www-m3.ma.tum.de/bornemann/inpainting.pdf`.
[3] Masnou, S. and Morel, J.-M.: Level lines based disocclusion, *ICIP '98: Proc. IEEE Int. Conf. on Image Processing, Chicago*, IEEE Press, New York (1998), pp. 259–263.
[4] Telea, A.: An image inpainting technique based on the fast marching method, *J. Graphics Tools* **9** (2004), pp. 23–34.

Regularization with Singular Energies: Error Estimation and Numerical Analysis

Martin Burger

(joint work with Elena Resmerita and Lin He)

Regularization with singular energies (being nonsmooth and not strictly convex) has become a standard tool in image processing and inverse problems over the last years. Famous examples are total variation methods (cf. [7]) and wavelet regularization in Besov scales, which is equivalent to wavelet shrinkage techniques (cf. [4, 5]). The transition from classical smooth regularization energies to singular ones offers enormous potential as we show in this talk. E.g. one can preserve or enhance certain structures such as sparsity with respect to some wavelet basis or sharp edges in total variation.

On the other hand, singular energies create an enormous challenge with respect to the analysis and discretization of the methods, many standard concepts such as norm convergence and norm estimation fail. As a useful tool for error estimation, so-called *generalized Bregman distances* have been introduced recently (cf. [2]). For a convex functional $J : X \to \mathbb{R} \cup \{+\infty\}$ (on a Banach space X) and a subgradient $p \in \partial J(u)$ a generalized Bregman distance is defined via

$$(1) \qquad D_J^p(v, u) = J(v) - J(u) - \langle p, v - u \rangle.$$

For a variational problem of the form

$$(2) \qquad \frac{\lambda}{2} \|Au - f\|^2 + J(u) \to \min_{u \in X},$$

it is remarkably easy to derive error estimates between the minimizer u_λ and the solution $\hat{u}$ of $A\hat{u} = g$, if $\hat{u}$ satisfies an additional smoothness condition of the form $q \in \partial J(\hat{u}) \cap \mathcal{R}(A^*)$. The error estimate for the Bregman distance (cf. [2]) is of the form

$$(3) \qquad D_J^q(u_\lambda, \hat{u}) = \mathcal{O}(\lambda^{-1} + \lambda \|f - g\|^2).$$

Such an error estimate holds in the case of a multivalued subgradient $\partial J(\hat{u})$, which is indeed typical for singular energies, for any subgradient satisfying the smoothness condition. More difficult seems the interpretation of such error estimates in special cases. However, it can be shown (also using multivaluedness of subgradients) that the Bregman distances yield indeed information about particularly interesting features, e.g. sparsity measures for wavelet shrinkage and difference of edges for total variation methods. Extensions of the approach to other schemes such as scale space or inverse scale space methods are possible (cf. [3]).

As an example of numerical schemes we consider the discretization of the ROF-model for total variation denoising respectively cartoon extraction (cf. [7])

$$(4) \qquad \frac{\lambda}{2} \int_\Omega (u - f)^2 + |u|_{TV} \to \min_{u \in BV(\Omega)}$$

by piecewise constant functions. It is well-known in this case (cf. [6] that direct discretizations of the variational problem do not converge in multiple spatial dimensions. We therefore propose a mixed discretization using piecewise constant functions for the primal and suitable elements for the dual variable (the subgradient respectively an associated vector field). This leads to a mixed discretization with a simple primal equation and a dual variational inequality (cf. [1]). Numerical analysis for such a scheme can again be carried out in terms of Bregman distances. This also provides information about certain finite difference schemes, which can be interpreted as versions of the mixed discretization on Cartesian grids.

References

[1] M. Burger, *Mixed discretization of total variation minimization problems*, in preparation.
[2] M.Burger, S.Osher, *Convergence rates for convex variational regularization*, Inverse Problems 20 (2004), 1411-1421.
[3] M. Burger, E. Resmerita, L. He, *Error estimation for Bregman iterations and inverse scale space methods in image restoration*, Preprint (2007).
[4] A. Chambolle, R. DeVore, N.Y. Lee, B. Lucier, *Nonlinear wavelet image processing: Variational problems, compression, and noise removal through wavelet shrinkage*, IEEE Trans. Image Proc., **7** (1998), 319–335.
[5] D.Donoho, I.Johnstone, *Ideal spatial adaptation via wavelet shrinkage*, Biometrika **81** (1994), 425–455.
[6] B.G.Fitzpatrick, S.L.Keeling, *On approximation in total variation penalization for image reconstruction and inverse problems*, Numer. Funct. Anal. Optimiz. **18** (1997), 941-958.
[7] L.I. Rudin, S.J. Osher, E. Fatemi, *Nonlinear total variation based noise removal algorithms*, Physica D **60** (1992), 259–268.

Some properties of the minimizers of the Total Variation. Application to surface evolution problems.

ANTONIN CHAMBOLLE

We have considered in this talk the celebrated "Rudin-Osher-Fatemi" image reconstruction problem, mathematically set as follows:

$$(1) \qquad \min_u \lambda \int_\Omega |Du| \; + \; \frac{1}{2} \int_\Omega (u(x) - f(x))^2 \, dx.$$

Here $u \mapsto \int_\Omega |Du|$ is the total variation of u and $f \in L^\infty(\Omega)$ represents the grey level of a noisy image, while the solution u of (1) is the denoised version; $\lambda > 0$ is a parameter which controls how much regularization is wanted and depends on the noise level. The total variation of a function is usually defined by duality:

$$\int_\Omega |Du| := \sup \left\{ \int_\Omega u \operatorname{div}\phi \, dx \, : \, \phi \in C_c^1(\Omega; \mathbb{R}^N) \, , |\phi(x)| \leq 1 \; \forall x \in \Omega \right\}$$

and the space of $u \in L^1(\Omega)$ with $\int_\Omega |Du| < +\infty$ is denoted by $BV(\Omega)$ (the functions with bounded variation in Ω).

The idea of using the total variation to regularize the inverse problem of finding u from the noisy observation f has been proposed first in this setting by Rudin,

Osher, and Fatemi in the early 90's, and corresponds to the fact that one wishes to take into account the spatial regularity of images, but also allow for the presence of sharp edges between different objects (which a more classical regularizing term like $\int_\Omega |\nabla u|^2$ would smear out).

This talk was about some applications of the following quite elementary result, which is proved in [8, 3] (see also [6]) and stated here as in [7].

Lemma 1. Let u solve (1). For any $t \in \mathbb{R}$, consider the minimal surface problem

$$(2) \qquad \min_{E \subseteq \Omega} \lambda P(E, \Omega) + \int_E (t - f(x)) \, dx$$

(whose solution is defined in the class of finite-perimeter sets, hence, up to a Lebesgue-negligible set). Then, $\{u_\lambda > t\}$ (respectively, $\{u_\lambda \geq t\}$) is the minimal (resp., maximal) solution of (2). In particular, for all t but a countable set, the solution of this problem is unique.

Here, $P(E, \Omega) := \int_\Omega |D\chi_E|$ is the perimeter of the set E in Ω (that is, roughly speaking, not counting $\partial E \cap \partial \Omega$). The proof of this lemma is based on the co-area formula which shows that

$$\lambda \int_\Omega |Du| + \frac{1}{2} \int_\Omega (u - f)^2 \, dx \sim \int \left(\lambda P(\{u > t\}, \Omega) + \int_{\{u > t\}} (t - f) \, dx \right) dt,$$

and on the following comparison result for solutions of (2) which is proved in [3, Lemma 4]:

Lemma 2. Let $f, g \in L^1(\Omega)$ and E and F be respectively minimizers of

$$\min_E P(E, \Omega) - \int_E f(x) \, dx \quad \text{and} \quad \min_F P(F, \Omega) - \int_F g(x) \, dx \, .$$

Then, if $f < g$ a.e., $|E \setminus F| = 0$ (in other words, $E \subseteq F$ up to a negligible set).

(The proof of this lemma is simple, it just relies on the inequality $P(A \cup B, \Omega) + P(A \cap B, \Omega) \leq P(A, \Omega) + P(B, \Omega)$ and is easily generalized to other situations such as Dirichlet boundary conditions, anisotropic and/or nonlocal perimeters, ..., see the proof in [3]).

In [7], in collaboration with V. Caselles and M. Novaga, we use this principle to deduce that if f in (1) is itself a BV function, with a jump set J_f (rectifiable, of codimension 1), then the BV function u solving (1) can only jump on a subset of J_f:

Theorem 1. *Let* $f \in BV(\Omega) \cap L^\infty(\Omega)$. *Then, for all* $\lambda > 0$,

$$(3) \qquad J_{u_\lambda} \subseteq J_f$$

(up to a set of zero $\mathcal{H}^{N-1}$*-measure, the Hausdorff measure of codimension 1).*

The proof of this result relies on standard regularity theory for the solutions of (2), as well as elliptic comparison results which show that solutions of (2) for different values of t can not "touch" too many times, at least where f does not

jump. Since the jump J_u of u is precisely where different level sets $\{u > t\}$ intersect (for at least two different values of t), the Theorem follows.

It also follows similar properties for the gradient flow of the total variation: if $u(t, x)$ solves

$$\begin{cases} \dfrac{\partial u}{\partial t} + \partial \displaystyle\int_\Omega |Du| \ni 0 & t > 0 \,, \\ u(0) = f & \text{in } \Omega \end{cases}$$

with $f \in L^\infty$, then $t > s \Rightarrow J_{u(t)} \subseteq J_{u(s)}$. This is a causality result: the flow cannot create edges where they were not already present at previous times (if the initial data is not itself BV, it does not say anything about the localization of the jumps at $t = 0^+$).

Let us mention that in a recent preprint, W. K. Allard also derived ¿from the same principle some regularity results for the solutions of (1)[1].

In the remaining part of the talk, other consequences of Lemma 1 were discussed, in particular from a numerical point of view. In particular, we have shown how (in the discrete setting) discrete variants of (1) are very efficiently solved, by a fast parametric max flow algorithm, by solving successive problems of type (2) and exploiting the monotonicity in Lemma 2. One shows that by performing J computations of a maximal flow over a suitable graph, one can solve the problem "exactly" up to a precision $(\max f - \min f) \cdot 2^{-J}$. This is a study in collaboration with Jérôme Darbon, and relies on previous studies of Gallo, Grigoriadis and Tarjan [12], Hochbaum [13], Boykov and Kolmogorov [4], Darbon and Sigelle [10, 11], see also [9]. Applications to surface evolution by crystalline curvature motion, following the algorithm of [2] and in the spirit of [5], were shown, in 2D and 3D.

References

[1] W. K. Allard. On the regularity and curvature properties of level sets of minimizers for denoising models using total variation regularization I: Geometric theory. *Submitted*, 2006.

[2] F. Almgren, J. E. Taylor, and L.-H. Wang. Curvature-driven flows: a variational approach. *SIAM J. Control Optim.*, 31(2):387–438, 1993.

[3] F. Alter, V. Caselles, and A. Chambolle. A characterization of convex calibrable sets in $\mathbb{R}^N$. *Math. Ann.*, 332(2):329–366, 2005.

[4] Y. Boykov and V. Kolmogorov. An experimental comparison of min-cut/max-flow algorithms for energy minimization in vision. *IEEE Trans. Pattern Analysis and Machine Intelligence*, 26(9):1124–1137, September 2004.

[5] Y. Boykov, V. Kolmogorov, D. Cremers, and A. Delong. An integral solution to surface evolution PDEs via Geo-Cuts. In A. Leonardis, H. Bischof, and A. Pinz, editors, *European Conference on Computer Vision (ECCV)*, volume 3953 of *LNCS*, pages 409–422, Graz, Austria, May 2006. Springer.

[6] V. Caselles and A. Chambolle. Anisotropic curvature-driven flow of convex sets. *Nonlinear Anal.*, 65(8):1547–1577, 2006.

[7] V Caselles, A. Chambolle and M. Novaga. The discontinuity set of solutions of the TV denoising problem and some extensions. Submitted.

[8] A. Chambolle. An algorithm for mean curvature motion. *Interfaces Free Bound.*, 6(2):195–218, 2004.

[9] A. Chambolle. Total variation minimization and a class of binary MRF models. In *Energy Minimization Methods in Computer Vision and Pattern Recognition*, Lecture Notes in Computer Science, pages 136–152, 2005.

[10] J. Darbon and M. Sigelle. Exact optimization of discrete constrained total variation minimization problems. In R. Klette and J. Zunic, editors, *Tenth International Workshop on Combinatorial Image Analysis*, volume 3322 of *LNCS*, pages 548–557, December 2004.

[11] J. Darbon and M. Sigelle. A fast and exact algorithm for total variation minimization. In J. S. Marques, N. Pérez de la Blanca, and P. Pina, editors, *2nd Iberian Conference on Pattern Recognition and Image Analysis*, volume 3522 of *LNCS*, pages 351–359, June 2005.

[12] G. Gallo, M. D. Grigoriadis, and R. E. Tarjan. A fast parametric maximum flow algorithm and applications. *SIAM J. Comput.*, 18(1):30–55, 1989.

[13] D. S. Hochbaum. An efficient algorithm for image segmentation, Markov random fields and related problems. *J. ACM*, 48(4):686–701 (electronic), 2001.

Topological persistence

DAVID COHEN-STEINER

(joint work with Herbert Edelsbrunner and John Harer)

Topological persistence, introduced by H. Edelsbrunner, D. Letscher and A. Zomorodian in 2000, is a way to distinguish "signal" from "noise" in a real function f defined over a topological space. The idea of persistence is to analyse the evolution of the topology of the sub-level-sets $f^{-1}(-\infty, x]$ as the threshold x increases. It turns out that this evolution can be encoded as a set of intervals, called *persistence intervals*. Each such interval represents the "life-span" of a topological event in the evolution of the sub-level-sets of f. As we will see, short intervals are usually induced by noise, whereas long ones witness the presence of a signal. An appealing aspect of topological persistence is that persistence intervals can be computed using a very simple and elegant algorithm in the case of piecewise-linear functions.

A key property of topological persistence is its stability against perturbations: when f is corrupted by a small amount of noise, its persistence intervals cannot change by much [1]. This property has several geometric consequences, depending on the function considered. It leads for example to a provable method for estimating the topology of an object from a cloud of sample points. It also yields new approximation results for the length of curves and for the total mean curvature of closed surfaces [2].

REFERENCES

[1] D. Cohen-Steiner, H. Edelsbrunner, J. Harer, *Stability of Persistence Diagrams*, to appear in *Disc. Comput. Geom.*

[2] D. Cohen-Steiner, H. Edelsbrunner, *Inequalities for the Curvature of Curves and Surfaces*, to appear in *J. FoCM*.

A variational model for optical flow and its relaxation

Sergio Conti

(joint work with Martin Rumpf)

In low level image processing, the accurate computation of object motion in scenes is a long standing problem, which has been addressed extensively. We consider an image sequence given via a grey-value map

$$u : [0, T] \times \Omega \to \mathbb{R}; \quad (t, x) \mapsto u(t, x)$$

on a space-time domain $D := [0, T] \times \Omega$, where Ω is a bounded Lipschitz domain in $\mathbb{R}^d$ for $d = 1, 2, 3$. If image points move according to a velocity field $v : D \mapsto \mathbb{R}^d$, and gray values $u(t, x(t))$ are constant along motion trajectories $x(t)$, one obtains the transport equation

$$(1) \qquad 0 = \frac{\mathrm{d}}{\mathrm{d}t} u(t, x(t)) = \partial_t u(t, x) + \nabla_x u(t, x(t)) \cdot v(t, x(t)),$$

as a constraint equation for the unknown velocity field v, the so-called brightness-constancy constraint. This condition gives us pointwise one constraint for d unknowns velocity components. Indeed, only the component of the velocity orthogonal to gray-value structures can be computed from Equation (1), which leads to an illposed problem known as the aperture problem. In the case that variations of the velocity field are on a spatial scale larger than the one for variations of the intensity field this can be solved via the so-called *structure tensor approach.*

We propose here a variational formulation which jointly segments the velocity and the intensity field, within a total variation framework as proposed for image denoising by Rudin, Osher and Fatemi [5]. Let us emphasize that in applications the reliable motion field extraction significantly benefits from a proper segmentation and vice versa. Precisely, given noisy data $u_0 : [0, T] \times \Omega \mapsto \mathbb{R}$, we propose to determine u and v by minimizing the functional

$$(2) \qquad E_0[u, v, D] = \int_D \left[|u - u_0|^2 + |\nabla v| + |\nabla u| + |(1, v) \cdot \nabla u| \right] \, dx.$$

Here and below, we write $\nabla = (\partial_t, \nabla_x)$ for the space-time gradient. This generalizes previous work by Aubert and Kornprobst [2] and Aubert, Deriche and Kornprobst [1], who considered a similar variational problem in the velocity field v alone, assuming the intensity u given. They already recognized that the last term is ill-defined in the presence of joint jumps in u and v, and proposed to replace E_0 with its relaxation in v (at constant u). In the numerical computations in [1] the problem was eliminated assuming the intensity field u to be Lipschitz continuous.

We propose instead to consider E_0 as a joint functional of u and v, which should be determined simultaneously. We present an analysis of the relaxation of the functional E_0 given in (2), including an explicit solution for the cell problem in one spatial dimension; numerical investigations are in progress. The key observation is that E_0 is not lower semicontinuous with respect to the relevant topology
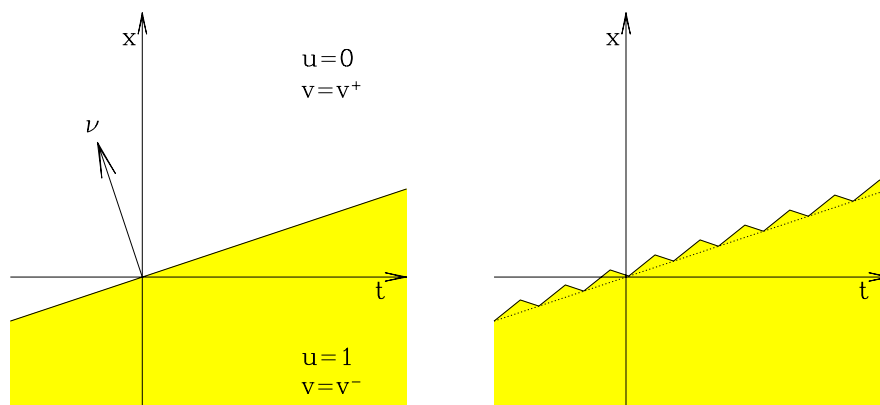
FIGURE 1. For relatively high velocities straight interfaces are unstable in the functional E_0 defined in (2), and spurious fine-scale oscillations are spontaneously formed, both in the velocity and in the intensity fields. This means that E_0 prefers the pattern on the right over the one on the left. The relaxed functional E^* does not suffer from this problem.

(weak convergence in BV). This can be best understood with a simple example, in which the data u_0 contain a single jump moving with constant velocity ξ, such as, e.g., $u_0 = \chi_{\{x \leq \xi t\}}$, and the velocity field takes two constant values v^+ and v^- on the two sides of the interface. Then for some range of values of the parameters v^+, v^- and ξ, minimizing sequences for E_0 spontaneously develop fine-scale oscillations, as illustrated in Figure 1. The scale of the oscillations is arbitrarily small in the continuum model, and would be set by the grid size in numerical computations. This difficulty can be solved by resorting to a relaxed formulation. Indeed, by replacing the functional by its lower semicontinuous envelope one obtains a problem where such oscillations are absent from the kinematics, but their energy is correctly accounted for in the functional; in the case at hand the relaxed formulation corresponds to attributing to the straight interface an energy which is smaller than that of all corresponding oscillatory interfaces.

Determining the relaxation of a functional corresponds to taking a lower semi-continuous envelope with respect to a topology under which the functional is coercive, which in this case is the weak BV topology. By the compact embedding of $BV \cap L^\infty$ into L^2 the fidelity term is continuous and we can focus on the reduced functional

$$(3) \qquad E[u, v, D] = \int_D \left[|\nabla v| + |\nabla u| + |(1, v) \cdot \nabla u| \right] \, dx$$

defined over the space $X = \left\{ (u, v) \in W^{1,1}(D, \mathbb{R}^{d+1}) : \|u\|_{L^\infty} + \|v\|_{L^\infty} \leq k \right\}$ where $k > 0$ is a real parameter. By general results by Fonseca and Müller [3, 4], its

relaxation has the form

$$E^*[u, v, D] = \begin{cases} \displaystyle\int_D \left[|\nabla v| + |\nabla u| + |(1, v) \cdot \nabla u| \right] dx + \int_{J_{(u,v)}} K(u^+, v^+, u^-, v^-, \nu)\, d\mathcal{H}^d \\ \qquad\qquad\qquad\qquad\qquad \text{if } u, v \in BV; \|u\|_{L^\infty} + \|v\|_{L^\infty} \leq k, \\ \infty \qquad\qquad\qquad\qquad\qquad\qquad\qquad\qquad\qquad \text{otherwise.} \end{cases}$$

Here we treat (u, v) as a vectorial BV function in defining the trace. This means, we denote by ν the normal to the rectifiable set $J_{(u,v)}$; given the orientation of the normal, u^+ and v^+ are defined as the traces on the side ν points to.

The surface energy K depends on the normal ν to the jump set and on the traces $u^\pm$, $v^\pm$, and is defined by a cell problem on the cube

$$Q_\nu = \{ x : |x \cdot \nu| < 1/2, |x \cdot \nu_i| < 1/2, i = 1, 2....d \},$$

where $(\nu, \nu_1, ... \nu_d)$ form an orthonormal basis of $\mathbb{R}^{d+1}$. Precisely,

$$K(u^+, v^+, u^-, v^-, \nu) = \inf \{ E[u, v, Q_\nu] : (u, v) \in \mathcal{A} \}$$

where $\mathcal{A}$ is the set of functions which are 1-periodic in the directions ν_i and agree with $u^\pm$, $v^\pm$ on the two sides of Q_ν normal to ν, in the sense of traces. We obtain the following characterization of K.

Theorem 2. *If $d = 1$, and $|u^+ - u^-| \leq 2$, the optimal energy is given by the following.*

If $\nu \cdot (1, v^-)$ and $\nu \cdot (1, v^+)$ have different sign, then

$$K(u^+, v^+, u^-, v^-, \nu) = |[u]| + |[v]|.$$

If they have the same sign, then

$$K(u^+, v^+, u^-, v^-, \nu) = \min_{\nu^+ \in \mathbb{R}^2} \psi(\nu^+),$$

where

$$\psi(\nu^+) = (|[u]| + |[v]|)(|\nu^+| + |\nu - \nu^+|) + |[u]|(|\nu^+ \cdot w^+| + |(\nu - \nu^+) \cdot w^-|).$$

In the latter case, the interface is one-dimensional if and only if the minimum is attained by $\nu^+ \in \{0, \nu\}$; in turn, this is equivalent to

$$(|[u]| + |[v]|)|\nu_2| \geq \frac{1}{2}|[u]|\,|[v]|.$$

REFERENCES

1. G. Aubert, R. Deriche, and P. Kornprobst, *Computing optical flow via variational techniques*, SIAM J. Appl. Math. **60** (1999), 156–182.
2. G. Aubert and P. Kornprobst, *A mathematical study of the relaxed optical flow problem in the space bv(ω)*, Siam J. Math. Anal. **30** (1999), 1282–1308.
3. I. Fonseca and S. Müller, *Quasi-convex integrands and lower semicontinuity in L^1*, SIAM J. Math. Anal. **23** (1992), 1081–1098.
4. ———, *Relaxation of quasiconvex functionals in* BV$(\Omega, \mathbb{R}^p)$ *for integrands $f(x, u, \nabla u)$*, Arch. Rational Mech. Anal. **123** (1993), 1–49.
5. L. Rudin, S. Osher, and E. Fatemi, *Nonlinear total variation based noise removal algorithms*, Physica D **60** (1992), 259–268.

Level Set Methods for 3D Reconstruction from Multiple Views

Daniel Cremers

(joint work with Kalin Kolev, Thomas Brox, Hailin Jin, Anthony Yezzi, and Stefano Soatto)

The reconstruction of three-dimensional objects from a collection of calibrated two-dimensional images of a scene is one of the fundamental problems in computer vision. Mathematically it is a highly ill-posed problem, much information is lost in the projections from 3D to 2D. As a consequence, there generally exists an entire family of 3D objects which are consistent with a given set of 2D images. Additional regularity assumptions need to be imposed in order to allow for unique solutions.

The reconstruction can be solved by minimizing cost functionals of the form

$$E(S) = E_{reconstruction}(S) + \alpha\, E_{regularity}(S)$$

over the space of closed regular surfaces $S \subset \mathbb{R}^3$, where $E_{reconstruction}$ measures the consistency of the surface S with the given set of 2D projections, while $E_{regularity}$ imposes regularity (for example smoothness) of the surface, weighted by a parameter $\alpha > 0$. Minimization can be done in a variational framework. The resulting 3D shape optimization problem can be solved using the level set method, i.e. the surface $S(t)$ at time t is represented implicitly as the zero-level of an embedding function $\phi : \mathbb{R}^3 \times [0, T] \rightarrow \mathbb{R}$:

$$S(t) = \{x \in \mathbb{R}^3 \mid \phi(x, t) = 0\}$$

and is propagated by evolving ϕ according to an appropriate partial differential equation — see the example in Figure 1.

Over the last years, numerous level set methods for multiview reconstruction have been proposed. Typically the respective data terms are based on stereo point correspondence computed between pairs or sets of images [1], or – alternatively – on the direct estimation of a consistent model of the surface intensity [2]. Stereo information is typically captured by estimating the normalized cross correlation over local patches thereby factoring out the object's intensity from the estimation problem. In contrast, the simultaneous estimation of the surface shape and intensity typically leads to more challenging infinite-dimensional optimization problems.
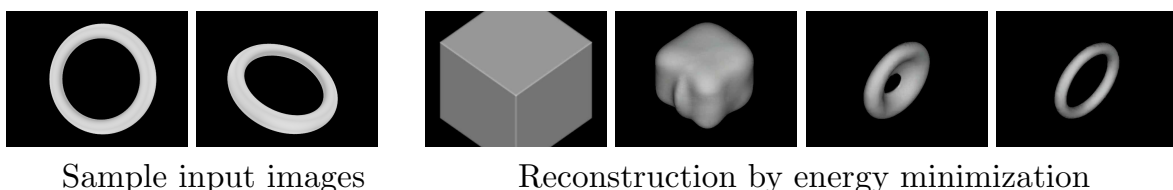

Sample input images   Reconstruction by energy minimization

FIGURE 1. 3D reconstruction from multiple views by local optimization of a respective cost functional [4].

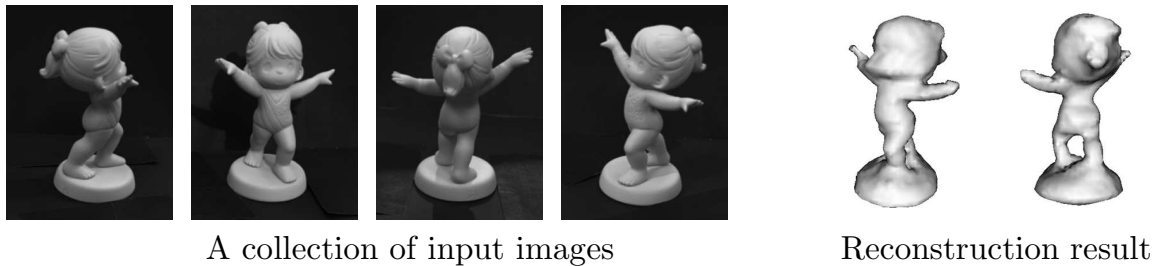A collection of input images   Reconstruction result

FIGURE 2. Joint estimation of 3D shape and illumination [3].

In my presentation, I will introduce the problem of multiview reconstruction, I will review a number of classical approaches and present some recent developments. In particular, I will show that one can model the physical image formation process by simultaneously estimating both the object shape, the object albedo and the incident illumination which gives rise to shading effects and cast shadows — see the example in Figure 2. Moreover, I will present probabilistic formulations of the reconstruction problem which aim at computing the most likely partioning of the volume given all observed images — see the example in Figure 3.
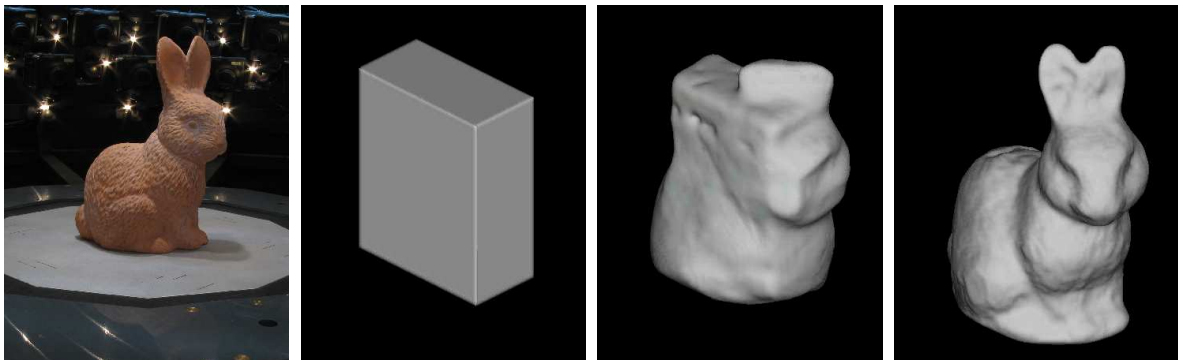
FIGURE 3. Probabilistic formulation of 3D Reconstruction [5].

REFERENCES

[1] O. Faugeras, and R. Keriven. *Variational principles, surface evolution, PDEs, level set methods, and the stereo problem.* IEEE Trans. on Image Processing, 7(3): 336–344, 1998.
[2] A. Yezzi, S. Soatto. *Stereoscopic segmentation.* International Journal of Computer Vision, 53(1):31–43, 2003.
[3] H. Jin, D. Cremers, A. Yezzi, and S. Soatto. *Sheding light on stereoscopic segmentation.* In L. Davis (editor), IEEE Int. Conf. on Computer Vision and Pattern Recognition, volume 1, pp. 36–42, Washington, DC, 2004.
[4] K. Kolev, T. Brox, and D. Cremers. *Robust variational segmentation of 3D objects from multiple views.* In K. Franke et al. (editor), Pattern Recognition (Proc. DAGM), volume 4174 of LNCS, pp. 688–697, Berlin, Germany, September 2006.
[5] K. Kolev, T. Brox, and D. Cremers. *Propagating Photoconsistency in Multiview 3D Reconstruction.* IEEE Int. Conf. on Computer Vision and Pattern Recognition 2007, submitted.

Finite elements on evolving surfaces

Charlie Elliott

1. Introduction

Partial differential equations on evolving surfaces occur in many applications. For example, traditionally they arise naturally in fluid dynamics and materials science and more recently in the mathematics of images. In this talk we describe a mathematical approach to the formulation and approximation of transport and diffusion of a material quantity on an evolving surface in $\mathbb{R}^{n+1}$ (n=1,2). We have in mind a surface which not only evolves in the normal direction so as to define the surface evolution but also has a tangential velocity associated with the motion of material points in the surface which advects material quantities such as heat or mass. For our purposes here we assume that the surface evolution is prescribed. This is joint work with G. Dziuk, [8, 9, 10, 11].

1.1. **The advection diffusion equation.** Conservation of a scalar with a diffusive flux on an evolving hypersurface $\Gamma(t)$ leads to the diffusion equation

$$\dot{u} + u\,\nabla_\Gamma \cdot v - \nabla_\Gamma \cdot (\mathcal{D}_0 \nabla_\Gamma u) = 0 \tag{1}$$

on $\Gamma(t)$. Here $\dot{u}$ denotes the covariant or advective surface material derivative, v is the velocity of the surface and ∇_Γ is the tangential surface gradient. If $\partial\Gamma(t)$ is empty then the equation does not need a boundary condition. Otherwise we can impose Dirichlet or Neumann boundary conditions on $\partial\Gamma(t)$.

1.2. **Applications.** Such a problem arises, for example, when modeling the transport of an insoluble surfactant on the interface between two fluids, [18, 14]. Here one views the velocity of the surface as being the fluid velocity and hence the surfactant is transported by advection via the tangential fluid velocity (and hence the tangential surface velocity) as well by diffusion within the surface. The evolution of the surface itself in the normal direction is then given by the normal component of the fluid velocity.

Diffusion induced grain boundary motion, [5, 12, 17, 6], has the feature of coupling forced mean curvature flow for the motion of a grain boundary with a diffusion equation for a concentration of mass in the grain boundary. In this case there is no material tangential velocity of the grain boundary so it is sufficient to consider the surface velocity as being in the normal direction.

Another example is pattern formation on the surfaces of growing organisms modelled by reaction diffusion equations, [16]. Possible applications in image processing are suggested by the article [15].

2. Evolving Surface Finite Element Method (ESFEM)

The finite element approximation is based on the variational form

$$\frac{d}{dt}\int_{\Gamma(t)} u\varphi + \int_{\Gamma(t)} \mathcal{D}_0 \nabla_\Gamma u \cdot \nabla_\Gamma \varphi = \int_{\Gamma(t)} u\dot{\varphi} \tag{2}$$

where φ is an arbitrary test function defined on the surface $\Gamma(t)$ for all t. This provides the basis of our evolving surface finite element method (ESFEM) which is applicable to arbitrary evolving n–dimensional hypersurfaces in $\mathbb{R}^{n+1}$ (curves in $\mathbb{R}^2$) with or without boundary. Indeed this is the extension of the method of Dziuk [7] for the Laplace-Beltrami equation on a stationary surface. The principal idea is to use a polyhedral approximation of Γ based on a triangulated surface. It follows that a quite natural local piecewise linear parameterisation of the surface is employed rather than a global one. The finite element space is then the space of continuous piecewise linear functions on the triangulated surface whose nodal basis functions enjoy the remarkable property

$$\dot{\phi}_j = 0.$$

The implementation is thus rather similar to that for solving the diffusion equation on flat stationary domains. For example, the backward Euler time discretization leads to the ESFEM scheme

$$\frac{1}{\tau}\left(\mathcal{M}(t^{m+1})\alpha^{m+1} - \mathcal{M}(t^m)\alpha^m\right) + \mathcal{S}(t^{m+1})\alpha^{m+1} = 0$$

where $\mathcal{M}(t)$ and $\mathcal{S}(t)$ are the time dependent surface mass and stiffness matrices and α^m is the vector of nodal values at time t^m. Here, τ denotes the time step size.

3. Level set or implicit surface approach

We also define an Eulerian level set method for parabolic partial differential equations on an evolving hypersurface $\Gamma(t)$ contained in a domain $\Omega \subset \mathbb{R}^{n+1}$. The method is based on formulating the partial differential equations on all level set surfaces of a prescribed time dependent function Φ whose zero level set is $\Gamma(t)$. Eulerian surface gradients are formulated by using a projection of the gradient in $\mathbb{R}^{n+1}$ onto the level surfaces of Φ. These Eulerian surface gradients are used to define weak forms of surface elliptic operators and so generate weak formulations of surface elliptic and parabolic equations. The resulting equation is then solved in one dimension higher but can be solved on a mesh which is unaligned to the level sets of Φ. We consider both second order and fourth order elliptic operators with natural second order splittings. The finite element method is applied to the weak form of the split system of second order equations using piece-wise linear elements on a fixed grid yielding an Eulerian ESFEM. The computation of the mass and element stiffness matrices are simple and straightforward.

3.1. **Eulerian conservation and diffusion.** Let $\Phi : \Omega_T \to \mathbb{R}$ be a prescribed non-degenerate level set function. Let $Q : \Omega_T \to \mathbb{R}^{n+1}$ be a given flux. Then the Eulerian conservation law we consider is

$$(3) \qquad \frac{d}{dt}\int_R u|\nabla\Phi| = -\int_{\partial R}(Q + |\nabla\Phi|uv)\cdot\nu_{\partial R}$$

for each sub-domain R of Ω where ν_R is the outward unit normal to ∂R. In particular we consider a flux of the form

$$Q = |\nabla\Phi| q_\Phi$$

where $q_\Phi : \Omega_T \to \mathbb{R}^{n+1}$ is a flux satisfying

(4) $$q_\Phi \cdot \nu = 0.$$

It follows by an implicit surface Leibniz formula that

(5) $$\frac{d}{dt} \int_R u |\nabla\Phi| = \int_R (\dot{u} + u\nabla_\Phi \cdot v) |\nabla\Phi| - \int_{\partial R} uv \cdot \nu_{\partial R} |\nabla\Phi|$$

and by Eulerian integration by parts and (4) that

(6) $$\int_{\partial R} q_\Phi \cdot \nu_{\partial R} |\nabla\Phi| = \int_R \nabla_\Phi \cdot q_\Phi |\nabla\Phi|.$$

It follows that

$$\int_R |\nabla\Phi|(\dot{u} + u\nabla_\Phi \cdot v + \nabla_\Phi \cdot q_\Phi) = 0$$

for every sub-domain R which implies the partial differential equation

(7) $$\dot{u} + u\nabla_\Phi \cdot v + \nabla_\Phi \cdot q_\Phi = 0 \text{ in } \Omega.$$

Taking q_Φ to be the diffusive flux

(8) $$q_\Phi = -\mathcal{A}\nabla_\Phi u$$

leads to the diffusion equation

(9) $$\dot{u} + u\nabla_\Phi \cdot v - \nabla_\Phi \cdot (\mathcal{A}\nabla_\Phi u) = 0.$$

Here $\mathcal{A} \geq 0$ is a symmetric mobility tensor with the property that it maps the tangent space $\mathcal{T} = \{\nu^\perp \in \mathbb{R}^{n+1} : \nu \cdot \nu^\perp = 0\}$ into itself, so that

$$\mathcal{A}\nu^\perp \cdot \nu = 0 \,\, \forall \nu^\perp \in \mathcal{T}.$$

Observe that (9) is a linear degenerate parabolic equation because $\mathcal{P}_\Phi$ has a zero eigenvalue in the normal direction ν. Another form of this PDE, less suitable for numerical purposes than (9) is given as

$$u_t + V\frac{\partial u}{\partial \nu} + \nabla_\Phi \cdot (uv_S) - VH_\Phi u - \nabla_\Phi \cdot (\mathcal{A}\nabla_\Phi u) = 0.$$

The variational form of (9) is obtained in the following way. For each level surface of Φ we multiply equation (9) by a test function η and use the coarea formula to yield

(10) $$\int_\Omega (\dot{u} + u\nabla_\Phi \cdot v - \nabla_\Phi \cdot (\mathcal{A}\nabla_\Phi u)) \, \eta |\nabla\Phi| = 0.$$

Observe that the Leibniz formula, gives

$$\frac{d}{dt} \int_\Omega u\eta |\nabla\Phi| = \int_\Omega (\dot{u} + u\nabla_\Phi \cdot v) \, \eta |\nabla\Phi| + \int_\Omega u\dot{\eta} |\nabla\Phi| - \int_{\partial\Omega} u\eta v \cdot \nu_{\partial\Omega} |\nabla\Phi|$$

and integration by parts because of $\mathcal{A}\nabla_\Phi u \cdot \nu = 0$ gives

$$\int_\Omega \mathcal{A}\nabla_\Phi u \cdot \nabla_\Phi \eta |\nabla\Phi| = -\int_\Omega \eta \nabla_\Phi \cdot (\mathcal{A}\nabla_\Phi u)\,|\nabla\Phi| + \int_{\partial\Omega} \mathcal{A}\nabla_\Phi u \cdot \nu_{\partial\Omega}\eta|\nabla\Phi|.$$

In order to proceed we need a boundary condition for u on $\partial\Omega$. It is natural to impose the zero flux condition

$$(11) \qquad\qquad |\nabla\Phi|(\mathcal{A}\nabla_\Phi u + uv) \cdot \nu_{\partial\Omega} = 0 \text{ on } \partial\Omega.$$

Finally we obtain

$$(12) \qquad\qquad \frac{d}{dt}\int_\Omega u\eta|\nabla\Phi| + \int_\Omega \mathcal{A}\nabla_\Phi u \cdot \nabla_\Phi\eta|\nabla\Phi| = \int_\Omega u\dot\eta|\nabla\Phi|.$$

3.2. **Finite Element Approximation.**

3.2.1. *Semi-discrete Approximation.* Our Eulerian ESFEM is based on the the weak form of the diffusion equation. We use fixed in time finite element functions so that now the test functions now will satisfy $\dot\eta = v \cdot \nabla\eta$.

We assume that the domain Ω is triangulated by an admissible triangulation $\mathcal{T}_h = \bigcup_{T\in\mathcal{T}_h} T$ which consists of simplices T. The discrete space then is

$$S_h = \{U \in C^0(\overline\Omega)|\, U|_T \text{ is a linear polynomial}, T \in \mathcal{T}_h\}.$$

The discrete space is generated by the nodal basis functions χ_i, $i = 1, \ldots, N$,

$$S_h = \mathrm{span}\{\chi_1, \ldots, \chi_N\}.$$

It is possible to generalize the method to higher order finite elements.

Definition 3.1 (Semi-discretization in Space)**.** Find $U(\cdot, t) \in S_h$ such that

$$(1) \qquad \frac{d}{dt}\int_\Omega U\eta|\nabla\Phi| + \int_\Omega \mathcal{A}\nabla_\Phi U \cdot \nabla_\Phi\eta|\nabla\Phi| = \int_\Omega Uv \cdot \nabla\eta|\nabla\Phi| \quad \forall\eta \in S_h.$$

Using the Leibniz formula it is easily seen that an equivalent formulation is:

$$(2) \qquad \int_\Omega \dot U\eta|\nabla\Phi| + \int_\Omega U\eta\nabla_\Phi \cdot v|\nabla\Phi| + \int_\Omega \mathcal{A}\nabla_\Phi U \cdot \nabla_\Phi\eta|\nabla\Phi| = 0 \quad \forall\eta \in S_h.$$

Setting

$$U(\cdot, t) = \sum_{j=1}^N \alpha_j(t)\chi_j(\cdot, t)$$

we find that

$$\frac{d}{dt}\left(\int_\Omega \sum_{j=1}^N \alpha_j\chi_j\eta|\nabla\Phi|\right)$$

$$+ \int_\Omega \mathcal{A}\sum_{j=1}^N \alpha_j\nabla_\Phi\chi_j \cdot \nabla_\Phi\eta|\nabla\Phi| = \int_\Omega \sum_{j=1}^N \alpha_j\chi_j v \cdot \nabla\eta|\nabla\Phi|$$

forall $\eta \in S_h$ and taking $\eta = \chi_k$, $k = 1, \ldots, N$ we obtain

$$(3) \qquad \frac{d}{dt}\left(\mathcal{M}(t)\alpha\right) + \mathcal{S}(t)\alpha = \mathcal{C}(t)\alpha$$

where $\mathcal{M}(t)$ is the evolving mass matrix

$$\mathcal{M}(t)_{kj} = \int_\Omega \chi_j \chi_k |\nabla\Phi|,$$

$\mathcal{C}$ is a transport matrix

$$\mathcal{C}(t)_{kj} = \int_\Omega \chi_j v \cdot \nabla\chi_k |\nabla\Phi|,$$

and $\mathcal{S}(t)$ is the evolving stiffness matrix

$$\mathcal{S}(t)_{jk} = \int_\Omega \mathcal{A}\nabla_\Phi \chi_j \nabla_\Phi \chi_k |\nabla\Phi|.$$

Since the mass matrix $\mathcal{M}(t)$ is uniformly positive definite on $[0, T]$ and the other matrices are bounded, we get existence and uniqueness of the semi-discrete finite element solution.

Remark 3.2. A significant feature of our approach is the fact that the matrices $\mathcal{M}(t)$, $\mathcal{C}(t)$ and $\mathcal{S}(t)$ depend only on the evaluation of the gradient of the level set function Φ and the velocity field v. The method does not require a numerical evaluation of the curvature.

References

[1] D. Adalsteinsson and J. A. Sethian *Transport and diffusion of material quantities on propagating interfaces via level set methods* J. Computational Physics **185** (2003) 271–288.

[2] Th. Aubin *Nonlinear analysis on manifolds. Monge-Ampère equations* Springer Berlin-Heidelberg-New York (1982)

[3] M. Bertalmio, L. T. Cheng, S. Osher and G. Sapiro *Variational problems and partial differential equations on implicit surfaces* J. Comput. Phys. **174** (2001) 759–780.

[4] M. Burger *Finite element approximation of elliptic partial differential equations on implicit surfaces* CAM-Report 05-46 UCLA (2005)

[5] J. W. Cahn, P. Fife and O. Penrose *A phase field model for diffusion induced grain boundary motion* Acta Mater. **45** (1997) 4397–4413.

[6] K. Deckelnick, C. M. Elliott and V. Styles *Numerical diffusion induced grain boundary motion* Interfaces and Free Boundaries **3** (2001) 393-414.

[7] G. Dziuk *Finite Elements for the Beltrami operator on arbitrary surfaces* In: S. Hildebrandt, R. Leis (Herausgeber): Partial differential equations and calculus of variations. Lecture Notes in Mathematics Springer Berlin Heidelberg New York London Paris Tokyo **1357** (1988) 142–155.

[8] G. Dziuk and C.M. Elliott *Finite elements on evolving surfaces* IMAJ Num. Anal. Advance Access published on August 7, 2006. doi:10.1093/imanum/drl023

[9] G. Dziuk and C. M. Elliott *Surface finite elements for parabolic equations* J. Computational Maths (submitted)

[10] G. Dziuk and C. M. Elliott *Eulerian finite element method for parabolic equations on implicit surfaces* Interfaces and Free Boundaries (submitted)

[11] G. Dziuk and C. M. Elliott *Eulerian finite element method for parabolic PDEs on implicit surfaces* In preparation

[12] P. Fife, J. W. Cahn and C. M. Elliott *A free boundary model for diffusion induced grain boundary motion* Interfaces and Free Boundaries **3** (2001) 291–336.

[13] J. Greer, A. Bertozzi and G. Sapiro *Fourth order partial differential equations on general geometries* J. Computational Physics **216**(1) (2006) 216-246.

[14] A. J. James and J. Lowengrub *A surfactant-conserving volume-of-fluid method for interfacial flows with insoluble surfactant* Journal of Computational Physics **201** (2004) 685–722.

[15] Hailin Jin, A. J. Yezzi and S. Soatto *Region based segmentation on evolving surfaces with application to 3D reconstruction of shape and piecewise constant radiance* UCLA preprint (2004)

[16] C. H. Leung and M. Berzins *A computational model for organism growth based on surface mesh generation* J. Computational Physics **188** (2003) 75–99.

[17] U. F. Mayer and G. Simonnett *Classical solutions for diffusion induced grain boundary motion* J. Math. Anal. **234** (1999) 660–674.

[18] H. A. Stone *A simple derivation of the time-dependent convective-diffusion equation for surfactant transport along a deforming interface* Phys. Fluids A **2** (1990)111–112.

[19] Jian-Ju Xu and Hong-Kai Zhao *An Eulerian formulation for solving partial differential equations along a moving interface* J. Sci. Comput. **19** (2003) 573–594.

New models and algorithms for image processing

Selim Esedoḡlu

• **Shape priors in curve evolution based segmentation:** A considerable number of signatures for shape comparisons that are invariant under certain transformations have been proposed and utilized in previous work on computer vision; see e.g. references in [10]. An interesting problem is to identify signatures that are particularly convenient to incorporate into region based segmentation models and their level set based implementations. In joint work with Frederick Park, we propose one such invariant shape signature that emerged in conversations with Eitan Tadmor. It is based on the Radon transform of sets, and is invariant under rotations and translations.

Main Idea: For a shape represented by the set $\Sigma \subset \mathbb{R}^2$, compute the following function:

$$(1) \qquad \mathbf{A}_\Sigma(\mu) := \mathrm{Area}\left(\left\{(\tau, \theta) \; : \; (\mathcal{R}\mathbf{1}_\Sigma)(\tau, \theta) \leq \mu\right\}\right)$$

where $\mathcal{R}$ denotes the Radon transform. This shape prior can be regarded as the natural analogue of an important *joint invariant* of polygonal curves. Namely, the histogram (and hence the cumulative distribution function) of pairwise distances between the vertices of a polygonal curve is invariant under solid motions, and has been shown in [3, 2] to determine the placement of the vertices uniquely up to Euclidean motions, except for a negligible set of shapes. For convex shapes, our proposed signature (1) can be seen as a continuum analogue of the cumulative distribution function of pairwise distances between boundary points; indeed, for a given μ, it measures, in the (τ, θ)-space, the "amount" of line segments of length less than μ that can be drawn between the boundary points of the convex shape.

We use (1) as a shape prior in region based segmentation models such as the piecewise constant Mumford-Shah model [12]. In terms of a level set function $\phi(x)$

representing the set Σ, so that $\Sigma = \{x \: : \: \phi(x) \geq 0\}$), the proposed signature (1) can be expressed as follows:

$$\mathbf{A}_\Sigma(\mu) = \iint H\Big(\mu - \mathcal{R}\big(H(\phi)\big)\Big) \, d\tau \, d\theta$$

where $H(\xi)$ is the Heaviside function: $H(\xi) = 1$ if $\xi \geq 0$, and $H(\xi) = 0$ otherwise. This somewhat clumsy way of expressing (1) facilitates the computations below.

Given also a reference shape represented by a set $\Omega \subset \mathbb{R}^2$ and a corresponding level set function $\psi(x)$ so that $\Omega = \{x \: : \: \psi(x) \geq 0\}$, we can incorporate the following term in our segmentation models to encourage the model to look for shapes resembling Ω:

(2)
$$\mathbf{S}(\phi) := \int_\mathbb{R} \big(\mathbf{A}_{\{\phi \geq 0\}}(\mu) - \mathbf{A}_{\{\psi \geq 0\}}(\mu)\big)^2 \, d\mu$$

$$= \int_\mathbb{R} \left(\iint H\Big(\mu - \mathcal{R}\big(H(\phi)\big)\Big) - H\Big(\mu - \mathcal{R}\big(H(\psi)\big)\Big) \, d\tau \, d\theta\right)^2 \, d\mu$$

Gradient descent for (2) with respect to the level set function ϕ can now be computed in the standard way. One gets:

(3)
$$\phi_t(x,t) = |\nabla\phi|\mathcal{R}^*\Big\{\mathbf{A}_{\phi \geq 0}\big(\mathcal{R}(H(\phi))\big) - \mathbf{A}_{\psi \geq 0}\big(\mathcal{R}(H(\phi))\big)\Big\}$$

Here, $\mathcal{R}^*$ is the adjoint of the Radon transform (i.e. the back projection operator). Equation (3) is a particularly clean expression that can be easily incorporated into conventional segmentation models:

● **New Directions in Diffusion Generated Motion:** The original diffusion generated motion algorithm was proposed by Merriman, Bence, and Osher (MBO) in [11]. It approximates the motion by mean curvature of the boundary $\partial\Sigma$ of a set $\Sigma \subset \mathbb{R}^N$ at discrete times $n\delta t$ by alternating the convolution of $\mathbf{1}_\Sigma$ by a radially symmetric kernel and thresholding the result at $\frac{1}{2}$.

Recently in [7, 6], together with S. Ruuth and R. Tsai we worked on extending theshold dynamics to a number of high order interfacial motions, in which the normal velocity of the interface can depend on derivatives of its curvature, and explored applications to image processing tasks that require these motions, such as image inpainting [1, 5] and disocclusion. We were motivated by recent results of Grzibovskis and Heintz [8], who proposed an MBO style algorithm for generating a fourth order evolution known as *Willmore flow*. This is gradient descent for the energy

(4)
$$E(\Sigma) = \int_{\partial\Sigma} K^2 \, d\sigma$$

where K denotes the mean curvature of the surface $\partial\Sigma$, and $d\sigma$ denotes the surface area element.

A serious drawback of MBO style algorithms has always been their thresholding step. Thresholding leads to a binary representation of the interface on the computational grid. With such a representation, it is impossible to interpolate and locate the interface at subgrid resolution. Hence, accurate computations with

these algorithms have until now required the use of adaptive grid refinement and approximate FFT on non-uniform grids as developed by Ruuth in [13].

To devise highly accurate versions of diffusion generated motion on uniform grids, in joint work with S. Ruuth and R. Tsai, we propose replacing the thresholding step that appears in these algorithms. Our proposal is to represent the interface using the *signed distance function*. The immediate advantage is that $d_{\partial\Sigma}(x)$ is Lipschitz continuous, and allows for interpolation to locate the interface with subgrid accuracy on a uniform grid. Moreover, there are already highly accurate and very efficient algorithms for computing the distance function. The essential question now becomes whether interesting motions can be generated by alternating the construction of the signed distance function, and its convolution with a kernel (or, more generally, making it the initial condition of a linear parabolic PDE). To that end we carried out the following preliminary analysis.

Let the signed distance function to the boundary $\partial\Sigma$ be denoted $d(x, y)$, so that $d > 0$ in Σ, and $d < 0$ outside. Assume that the curve $\partial\Sigma$ is tangent to the x-axis at the origin with outer normal pointing in the $(0, -1)$ direction, and that $\partial\Sigma$ is given by the graph of a function $f(x)$. We have obtained the following expansion for $d(x, y)$ near the origin, in terms of the geometry of the curve $\partial\Sigma$:

$$(5)\quad d(x, y) = y + \frac{1}{2}Kx^2 + \frac{1}{6}\big(K'x^3 - 3K^2x^2y\big)$$
$$+ \frac{1}{24}\Big(\big(K'' - 3K^3\big)x^4 - 12KK'x^3y + 12K^3x^2y^2\Big) + o(r^4).$$

Using (5), we found the following expansion for the convolution of d with the Gauss kernel:

$$(6)\qquad (G_t * d)(0, y) = y + Kt - K^2ty + \frac{1}{2}\big(K'' + K^3\big)t^2 + o(t^2).$$

Using (6), we can now design algorithms that alternate construction of the signed distance function and its convolution with kernels. A very simple example is motion by mean curvature, which can be obtained by alternating convolution with the Gaussian kernel with redistancing (see [4, 9] for related work); this can be seen by concentrating on the two lowest order in t terms of the expansion (6).

Of course, that motion by mean curvature results form the algorithm above is not surprising: after all, convolution with the Gauss kernel is equivalent to the solution of the heat equation, and Laplacian of the signed distance function gives mean curvature of the level sets. However, we can use expansions (5) and (6) to design more interesting algorithms; an example is:

Distance function based, diffusion generated Willmore flow: By manipulating expansion (6), the following algorithm is seen to approximate the Willmore flow of $\partial\Sigma \subset \mathbb{R}^2$ at the discrete times $n\delta t$:

(1) Given $d_{\partial\Sigma^n}(x)$, form the following function:

$$p(x) = \big(2G_{\sqrt{\delta t}} - G_{2\sqrt{\delta t}}\big) * d_{\Sigma^n} + \frac{1}{2}\big(G_{\delta t^{\frac{1}{3}}} * d_{\Sigma^n} - d_{\Sigma^n}\big)^3.$$

(2) Reconstruct the distance function to the zero level set of $p(x)$ by solving:

$$u_t(x,t) = \text{sign}\big(p(x)\big)\big(1 - |\nabla u|\big) \text{ with } u(x,0) = p(x)$$

for large enough time T, and set $d_{\partial \Sigma^{n+1}} = u(x,T)$.

We expect this algorithm to have excellent stability properties so that large time steps can be taken.

References

[1] M. Bertalmio, G. Sapiro, V. Caselles, and C. Ballester. *Image inpainting.* ACM Siggraph Computer Graphics Proceedings. (2000), 417–424.

[2] M. Boutin and G. Kemper. *Which point configurations are determined by the distribution of their pairwise distances.* To appear in Int. J. Compt. Geometry and Appl (2006).

[3] M. Boutin and G. Kemper. *On reconstructing n-point configurations from the distribution of distances or areas.* Adv. Appl. Math. **32** (2004), 709–735.

[4] A. Chambolle. *An algorithm for mean curvature motion.* Interfaces and Free Boundaries. **6**:2 (2004), 195–218.

[5] T. Chan, J. Shen, and S. Kang. *Euler's elastica and cuvature based inpainting.* SIAM J. Appl. Math. **63**:2 (2002), 564–592.

[6] S. Esedoḡlu, S. Ruuth, and Y.-H. Tsai. *Threshold dynamics for high order geometric motions.* UCLA CAM Report 06-23 (2006). Submitted.

[7] S. Esedoḡlu, S. Ruuth, and Y.-H. Tsai. *Threshold dynamics for shape reconstruction and disocclusion.* Proceedings of the ICIP (2005).

[8] R. Grzibovskis and A. Heintz. *A convolution-thresholding scheme for Willmore flow.* Chalmers University of Technology Preprint no. 34. (2003).

[9] M. Kimura and H. Notsu. *A level set method using the signed distance function.* Japan J. Indust. Appl. Math. **19** (2003), 415–446.

[10] S. Manay, D. Cremers, B.-W. Hong, A. J. Yezzi, and S. Soatto. *Integral invariants for shape matching.* IEEE Transactions on Pattern Analysis and Machine Intelligence. **28**:10 (2006), 1602–1618.

[11] B. Merriman, J. K. Bence, and S. Osher. *Motion of multiple junctions: a level set approach.* J. Comput. Phys. **112**:12 (1994), 334–363.

[12] D. Mumford and J. Shah. *Optimal approximations by piecewise smooth functions and associated variational problems.* Comm. Pure. Appl. Math. **42** (1989), 577-685.

[13] S. Ruuth. *Efficient algorithms for diffusion-generated motion by mean curvature.* J. Comput. Phys. **14** (1998), 603–625.

On convolution-thresholding schemes for the Willmore and the generalised curvature flows and on homothetic geometric flows.

Alexei Heintz

(joint work with Richards Grzhibovskis, Tobias Gebäck)

Willmore flow is a surface Γ moving by normal velocity equal to

$$(1) \qquad W = - \big[\Delta H + 2H \big(H^2 - K\big)\big],$$

where H, K and ΔH are values of the mean curvature, the Gauss curvature and the Laplace-Beltrami operator of the mean curvature of Γ. By generalised mean curvature flow we mean a surface moving by normal velocity $g(H)$ where F is a

monotone function. We observe that the expression $\left(\Delta H + 2H\left(H^2 - K\right)\right)$ is the Euler operator of the Willmore functional $\int_\Gamma H^2 dS$.

   The problem of singularity formation in Willmore and curvature flows is discussed. We have found several new families of self-similar or homothetic solutions that either form a singularity in finite time starting from a smoooth initial surface or start from an initially singular surface that later transforms to a smooth surface. These particular solutions are used as a benchmark for our general numerical methods and are interesting for the theory of Willmore and curvature flows.

   We describe a general convolution-thresholding approach to approximation of the Willmore flow and the generalised curvature flows.

   Consider a bounded domain C in $\mathbb{R}^3$ with a smooth boundary ∂C. The main ingredient of our variant of the convolution-thresholding method is the connection between local geometric properties of ∂C and a new asymptotic expansion of the convolution

(2) $$M\left(\mathbf{r}\right) = \left(\chi_C \star \rho_{t^{1/4}}\right)\left(\mathbf{r}\right), \mathbf{r} \in \mathbb{R}^3,$$

in points $\mathbf{r}$ at the distance of order $O(t)$ from ∂C for $t \to 0$.

   Here χ_C is the characteristic function of C, $\rho_{t^\alpha}\left(\mathbf{r}\right) = \rho\left(\left|\mathbf{r}\right|^2 / t^{2\alpha}\right) / \left(t^\alpha\right)^3$. The function $\rho : (0, \infty) \mapsto [0, \infty)$ is smooth, has compact support (or exponentially decreasing) and is normalized by $\int_{R^3} \rho_1 d\mathbf{r} = 1$.

   $\mathbf{N}$ denotes later the external unit normal to ∂C at $\mathbf{p}$. The asymptotics of $M\left(\mathbf{r}\right)$ for $t \to 0$ is investigated in the point $\mathbf{r_0} = \mathbf{p} + \mathbf{N}vt$. Here $v \in \mathbb{R}$ and it has the sense of the normal velocity of the constructed geometric flow.

   Suppose ∂C is smooth, $\mathbf{p} \in \partial C$ and $v \in \mathbb{R}$, then the convolution (2) has the following asymptotic expansion with respect to $t \to 0$ at the point $\mathbf{r_0} = \mathbf{p} + \mathbf{N}vt$

$$M\left(\mathbf{r_0}\right) = \frac{1}{2} + t^{1/4}\frac{\pi N_3}{2}H \quad +$$
$$+t^{3/4}\frac{\pi}{16}\left[-32N_1 v + N_5\left(\Delta H + 2H\left(H^2 - K\right)\right)\right] \quad + \quad O\left(t^{5/4}\right)$$
(3)

where H, K and ΔH are values of the mean curvature, the Gauss curvature and the Laplace-Beltrami operator of the mean curvature of ∂C in the point $\mathbf{p}$ and $N_i = \int_0^\infty r^i \rho\left(r^2\right) dr$. We choose a linear combination of two convolutions as above with different weights ρ so that its zero level set moves as the Willmore flow of the suface ∂C. It leads to a convolution-thresholding approximation for the Willmore flow. Taking scaling $t^{1/2}$ instead of $t^{1/4}$ gives similar asymptotics as $t \to 0$ for M but with velocity v in the lower order term with mean curvature H. This scaling lets us approximate generalised curvature flows with velocity $v \equiv g(H)$ with monotone increasing function $g(H)$.

   The consistency of the method is justified for Willmore flows when the evolving surface is smooth. Numerical experiments show that the method performs well even in the case of non-smooth initial data. For generalised curvature flows the convergence of the method to viscosity solutions of the level set equations is proved for surfaces without boundaries and for the case with right angle condition in a
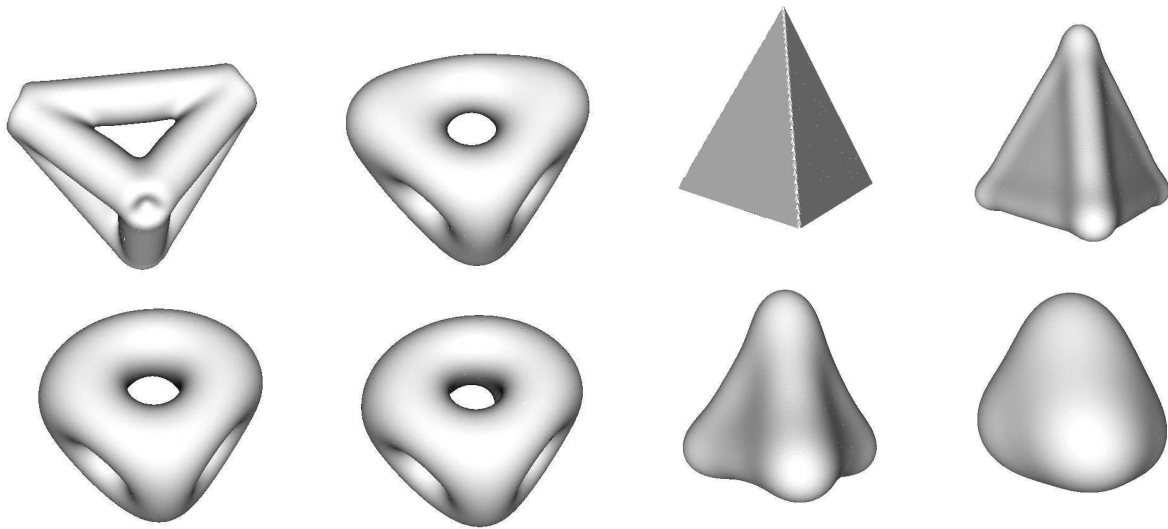
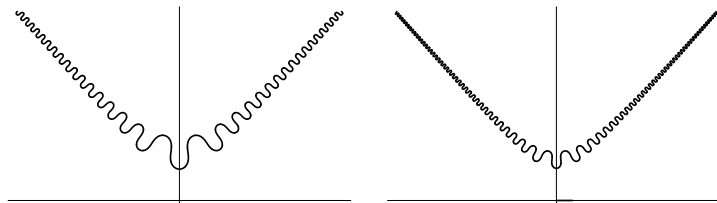FIGURE 1. The Willmore evolutions of a non-convex surface and of a pyramid.

FIGURE 2. Two smooth cylindrical surfaces that evolve self-similarly by the Willmore flow and develope an angle in finite time.

smooth domain. It corresponds to the Neumann boundary conditions for the level set equations.

REFERENCES

[1] R. GRZHIBOVSKIS AND A. HEINTZ, *A convolution-thresholding approximation of generalized curvature flows*, SIAM J. Numer. Anal.**42** (2005), 2652–2670.

[2] R. GRZIBOVSKIS AND A. HEINTZ *A convolution-thresholding scheme for the Willmore flow,* Chalmers Preprint **34** (2003),1–9.

[3] R. GRIZIBOVSKIS AND A. HEINTZ *On self-similar Willmore and curvature evolutions of surfaces* , Chalmers Preprint **29** (2004), 1–22

Isometry and Biometry

Ron Kimmel

(joint work with Alexander M. Bronstein and Michael M. Bronstein)

We focus on the problem of matching isometric manifolds by embedding their intrinsic geometric structures into simple (and less simple) domains. One obvious example goes back to expression invariant face recognition. In the talk we emphasize some theoretical problems and technical challenges, as well as recent advances like the generalized multidimensional scaling that we developed and use to embed for example one facial surface into another.

Generalized multidimensional scaling (GMDS) is an extension of traditional metric MDS, in which the target space is non-Euclidean. Particularly important setting of the problem is the isometric embedding problem, when one wishes to represent the intrinsic metric structure of one surface using the intrinsic geometry of another surface.

We developed an efficient theoretical and numerical framework for the solution of the GMDS problem. Using GMDS, many fundamental problems pattern analysis can be solved. First, GMDS allows to establish intrinsic geometric correspondence between two similar objects, e.g. two near-isometric deformations of the same object. Secondly, the average (or the maximum) metric distortion, referred to as "stress", serves as a measure of shape dissimilarity. Particularly, using GMDS it is possible to compute the Gromov-Hausdorff distance between two surfaces or the partial embedding distance, which allows for partial matching of surfaces. Finally, "local stress" obtained as a byproduct of the GMDS procedure allows to find local differences between two shapes.

We explore the use of the GMDS framework in applications such as 3D face recognition, expression-invariant texture for animated 3D facial surfaces, expression exaggeration, and face morphing.

Facial expressions, for example, can be modeled as isometries of the facial surface and Generalized MDS can then be used to establishing correspondence between two frames as an isometric embedding of one surface into another. This correspondence allows to map a single texture image in an expression-invariant manner to the frames of a 3D video of a face, creating a "virtual makeup" effect. Other applications include morphing between different faces, expression exaggeration and interpolation.

For further details see:

www.cs.technion.ac.il/∼mbron

www.cs.technion.ac.il/∼bron

www.cs.technion.ac.il/∼ron

Mean curvature of varifolds: locality and applications

Simon Masnou

(joint work with Gian Paolo Leonardi)

Varifolds were introduced by Almgren [2] and Allard [1] to generalize rectifiable manifolds in a way that allows multiplicity, ensures compactness and authorizes a generalized notion of mean curvature that is well posed even when singularities occur (see [11] for an exhaustive survey of the theory of varifolds). We recall that, given M a $\mathcal{H}^n$-rectifiable subset of $\mathbb{R}^{n+k}$ and θ a locally $\mathcal{H}^n$-integrable function on M representing a multiplicity function, the associated n-rectifiable varifold $V = \underline{\mathbf{v}}(M, \theta)$ has a first variation in U open subset of $\mathbb{R}^{n+k}$ that satisfies for every $X \in \mathrm{C}^1_c(U, \mathbb{R}^{n+k})$

$$\delta V(X) = \int_M \mathrm{div}_M \, X \theta d\mathcal{H}^n$$

where $\mathrm{div}_M \, X$ is the tangential divergence of X with respect to M. We are interested in those situations where the total variation $\|\delta V\|$ of δV is absolutely continuous with respect to $\mu := \theta \mathcal{H}^n \llcorner M$ and the generalized mean curvature

$$H(x) = (\lim_{r \to 0} \frac{\|\delta V\|(B_r(x))}{\mu(B_r(x))}) \nu(x)$$

is in $\mathrm{L}^p(\mu)$, with ν the generalized normal given by the Riesz representation theorem. In other words, we assume that for every $X \in \mathrm{C}^1_c(U, \mathbb{R}^{n+k})$,

$$\delta V(X) = -\int_M H \cdot X \, \theta d\mathcal{H}^n \quad \text{and} \quad \int_M |H|^p \theta d\mathcal{H}^n < +\infty$$

The motivation for this work comes from the study of the p-Willmore functional $\int_M |H|^p \theta d\mathcal{H}^n$, which appears in a large variety of problems in geometry, elasticity, biology, phase transitions and image processing. Concerning the specific case of image processing, the p-Willmore functional appears in the 2.1-D sketch of Mumford and Nitzberg [8, 5, 6, 4] and in the so-called inpainting problem [3, 7] in connection with the study of the relaxation of the functional

$$\int_\Omega |\nabla u|(1 + |\mathrm{div} \, \frac{\nabla u}{|\nabla u|}|^p) dx$$

A common issue raised in all these applications is the problem of the lower semi-continuity of the Willmore functional for integral varifolds, i.e. rectifiable varifolds with integer-valued multiplicity. As formulated by R. Schätzle [10], the problem is the following : take a converging sequence of integral n-currents $T_k \to T$ such that the associated integral varifolds V_{T_k} have bounded mean curvature in L^p and converge to a limit varifold V_∞. Then it is well known that

$$\|H_{\mu_\infty}\|_{\mathrm{L}^p(\mu_\infty)} \leq \liminf_{k \to \infty} \|H_{\mu_k}\|_{\mathrm{L}^p(\mu_k)}$$

where μ_∞, μ_k are the weights of the rectifiable varifolds V_∞, V_{T_k} and H_{μ_∞}, H_{μ_k} the associated mean curvatures. But it is not always clear whether

$$\|H_{\mu_T}\|_{\mathrm{L}^p(\mu_T)} \leq \liminf_{k \to \infty} \|H_{\mu_k}\|_{\mathrm{L}^p(\mu_k)}.$$

This inequality is actually true as soon as the locality of the mean curvature holds, i.e. $H_{\mu_T} = H_{\mu_\infty}$, μ_T-almost everywhere. However the locality is far from being a trivial problem due to the variational definition of the generalized mean curvature of varifolds. This problem can be formulated in the following form: let μ_1 and μ_2 be two integral n-varifolds such that $H_{\mu_1} \in \mathrm{L}^p(\mu_1)$ and $H_{\mu_2} \in \mathrm{L}^p(\mu_2)$. Is it true that for μ_1-a.e. x in $[\theta^{\star n}(\mu_1) > 0] \cap [\theta^{\star n}(\mu_2) > 0]$ it holds

$$H_{\mu_1}(x) = H_{\mu_2}(x) \quad ?$$

The state of the art for this problem is the following:

- Locality has been proved by L. Ambrosio and the author in [3] for any dimension $n \geq 2$, codimension $k = 1$ and integrability of the mean curvature $p > n$, $p \geq 2$. The proof is based on a crucial quadratic decay of the tilt-excess due to R. Schätzle [9]
- A much more general result due to R. Schätzle appears in [10]. The locality now holds in any dimension $n \geq 2$, any codimension, under the only assumption that the mean curvature is at least in $\mathrm{L}^2(\mu)$ and the varifold is C^2-rectifiable, i.e. $[\theta^{\star n}(\mu) > 0]$ can be covered by a countable union of C^2 n-submanifolds of $\mathbb{R}^{n+k}$. In particular, it is proved that if $H \in \mathrm{L}^2(\mu)$ then the C^2-rectifiability is equivalent to the quadratic decay of the height-excess and the tilt-excess.

The main difficulty for proving the locality at $x \in [\theta^{\star n}(\mu_1) > 0] \cap [\theta^{\star n}(\mu_2) > 0]$ is to control the parts of the varifolds μ_1, μ_2 that do not contribute in density to the multiplicity at x but may contribute to the mean curvature. Now the quadratic decay of the tilt-excess provides a local control on the whole varifold and not only on the parts with no contribution to the multiplicity. This let us think that, if we could avoid using a strong decay of the tilt-excess, then the assumption $H \in \mathrm{L}^2(\mu)$ could be weakened and the locality could hold assuming only that $H \in \mathrm{L}^1(\mu)$. We were actually able to prove the following results, which are optimal for 1-varifolds but only partial for n-varifolds, $n > 1$:

(1) The locality holds for integral 1-varifolds in any codimension assuming only that $H \in \mathrm{L}^1$;
(2) For $n > 1$, any codimension, the following partial proposition is true: if $V = \underline{\mathbf{v}}(M, \theta)$ is an integral n-varifold in $U \subset \mathbb{R}^{n+k}$ such that

$$
\begin{aligned}
&(i) \quad H_V \in \mathrm{L}^1(\mu_V),\\
&(ii) \quad M = N \cup S, \quad S \ \mathrm{C}^2 - \text{submanifold of } \mathbb{R}^{n+k},\\
&(iii) \quad \theta \text{ is piecewise constant on } S,
\end{aligned}
$$

then H_V and the classical mean curvature H_S coincide μ_V-almost everywhere on S.

The result for 1-varifolds, which is optimal, is based on the fact that $H \in \mathrm{L}^1$ is enough to ensure strong phenomena of compensation of the mean curvature within sufficiently many balls. The partial result for n-varifolds follows from the isoperimetric inequality and a control of the derivative of $\mu_V(N \cap B_r)$ with respect to r.

References

[1] W.K. Allard, *On the first variation of a varifold*, Annals of Math., **95** (1972), 417-491.

[2] F.J. Almgren, *The theory of varifolds*, Mimeographed notes, Princeton (1965).

[3] L. Ambrosio and S. Masnou, *A direct variational approach to a problem arising in image reconstruction*, Interfaces and Free Boundaries, **5**, no 1 (2003), 63-81.

[4] G. Bellettini, V. Beorchia and M. Paolini, *Topological and variational properties of a model for the reconstruction of three-dimensional transparent images with self-occlusions* (2006), submitted.

[5] G. Bellettini, G. Dal Maso and M. Paolini, *Semicontinuity and relaxation properties of a curvature depending functional in 2D*, Ann. Scuola Norm. Sup. Pisa, Cl. Sci (4),**20** (1993), 247-299.

[6] G. Bellettini and L Mugnai, *A varifolds representation of the relaxed elastica functional*, J. Convex Analysis (2007), to appear.

[7] S. Masnou, *Disocclusion: a variational approach using level lines*, IEEE Trans. Image Proc., **11** (2002), 68-76.

[8] M. Nitzberg and D. Mumford, *The 2.1-D sketch*, Proc. of the Third Int. Conf. on Comp. Vision, Osaka (1990).

[9] R. Schätzle, *Quadratic titl-excess decay and strong maximum principle for varifolds*, Ann. Scuola Norm. Sup. Pisa, Cl. Sci (5), **Vol. III** (2004), 171-231.

[10] R. Schätzle, *Lower semicontinuity of the Willmore functional for currents* (2004), submitted.

[11] L. Simon, *Lectures on geometric measure theory*, Proc. Centre for Math. Analysis, Austral. Nat. Univ., Camberra (1983).

A software code to manipulate apparent contours

Maurizio Paolini

(joint work with G. Bellettini, V. Beorchia and F. Pasquarelli)

Given a projection from a smooth compact surface Σ embedded in $\mathbb{R}^3$ onto $\mathbb{R}^2$, the corresponding apparent contour C is the set in $\mathbb{R}^2$ where the projection is not regular (at some preimage). Please note that since we require Σ to be embedded, it will also be orientable; we do not require Σ to be connected. If Σ is *generic*, its apparent contour consists in a collection of smooth oriented arcs (corresponding to folds of Σ) connecting a set of *crossings* and *cusps*. Each arc of the apparent contour can be augmented with a *depth* information (Huffman labelling [3]), which simply states how many layers of the surface lie ahead of the fold (Figure 1). With this labelling there is a unique way to recover the shape (up to a *vertical* deformation) of the originating surface Σ [2].

More general isotopic deformations of Σ will produce deformations in the apparent contour that undergo topological changes, as shown in Figure 1, where the torus on the left is slightly twisted in its upper-left part. The possible topology

FIGURE 1. Apparent contour of a torus before and after a deformation.

changes can be enumerated as a finite number of *rules*; two examples of such rules is presented in Figure 2. The complete set of rules can be found e.g. in [1].
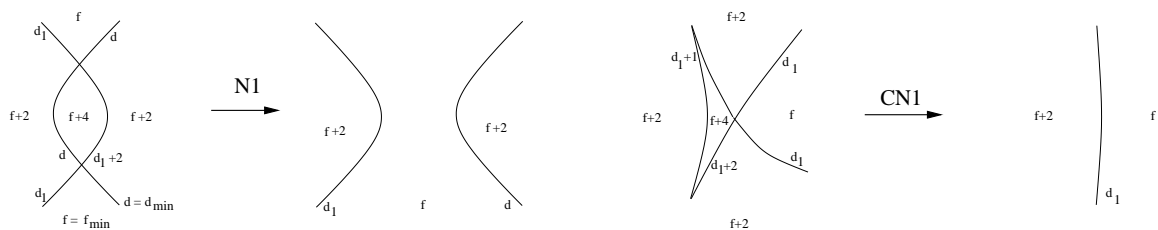

FIGURE 2. Rules n1 and cn1: disocclusion of a fold and removal of a swallowtail.

Applicability of each rule also depends on the orientation of the arcs involved and the local values of the depth function; checking by hand whether a rule can be applied or not, and producing the correct result can be tedious and error prone, hence the idea of developing a software code that automates such process.

The resulting software is named `appcontour` and is hosted on SourceForge (www.sourceforge.net). It relies on an internal representation of an apparent contour based on a description of the boundary of each *region* (connected component of the complement of the contour) in terms of the involved arcs and is capable of various manipulations, which includes listing the rules that can be applied and computing the result of the rule application. Some information on the originating surface such as the Euler characteristic and the number of connected components is also computed by the software.

A description of an apparent contour can be given in a more convenient way in a *Morse-theory* fashion by imagining a horizontal line traversing the contour from top to bottom and listing for all critical positions of the line the type and order of the intersections (possible types are: *transversal crossing*, *local maximum/minimum*, *cross point*).

Presentation of a resulting apparent contour is given in the form of a *region description*; a graphical 2D display can be obtained with an utility (*showcontour*) that produces a decent picture by smoothing up a polygonal that roughly represents the structure of the contour.

The source code of the software is available, and contributions are welcome, particularly for a graphical user interface, which is as yet missing; future development

can include extension of the code to treat apparent contours that are not coming from projections of embedded surfaces, such as nonoriented immersed surfaces (e.g. klein bottle and Boy surface) or even generic 2D manifolds with a smooth map in $\mathbb{R}^2$.

The above results have been obtained in collaboration with Giovanni Bellettini (Univ. Roma Tor Vergata, Italy) Valentina Beorchia (Univ. Trieste, Italy) and Franco Pasquarelli (Università Cattolica Brescia, Italy).

References

[1] F. Aicardi, T. Ohmoto, *First order local invariants of apparent contours*, Topology, **45** (2006), 27–45.

[2] G. Bellettini, V. Beorchia and M. Paolini, *Topological and variational properties of a model for the reconstruction of three-dimensional transparent images with self-occlusions*, Preprint Centro De Giorgi, 2006, submitted. Available at http://www.cvgmt.sns.it.

[3] D.A. Huffman, *Impossible objects as nonsense sentences*, in Machine Intelligence 6, B. Meltzer and D. Michie Eds., American Elsevier Publishing Co., New York 1971.

[4] O.A. Karpenko and J.F. Hughes, *SmoothSketch: 3D free-form shapes ¿from complex sketches*, Preprint 2006, to appear on Siggraph'06.

[5] D. Luminati, *Surfaces with assigned apparent contour*, Ann. Sc. Norm. Super. Pisa, Cl. Sci., IV. Ser. 21, **3** (1994), 311-341.

[6] R. Pignoni, *On surfaces and their contour*, Manuscripta Math., **72** (1991), 223-249.

[7] H. Whitney, *On singularities of mappings of euclidean spaces. I. Mappings of the plane into the plane*, Ann. of Math., **62** (1955), 374-410.

[8] L.R. Williams, *Topological reconstruction of a smooth manifold-solid from its occluding contour*, Int. J. Computer Vision, **23** (1997), 93–108.

Surface Parametrization - Guided by Curvature

Konrad Polthier

(joint work with Felix Kälberer and Matthias Nieser)

We introduce an algorithm for the automatic computation of a global parameterization on arbitrary simplicial 2-manifolds whose parameter lines are guided by a given frame field, for example, by principal curvature frames. The parameter lines are globally continuous and allow a remeshing of the surface into quadrilaterals.

The algorithm converts a given frame field into a single vector field on a branched covering of the 2-manifold and generates an integrable vector field by a Hodge decomposition on the covering space. Except an optional smoothing and alignment of the initial frame field, the algorithm is fully automatic and generates high quality quadrilateral meshes.

The algorithm [1] extends earlier work by [6] and has contact to the approaches of [3, 4, 5, 7]
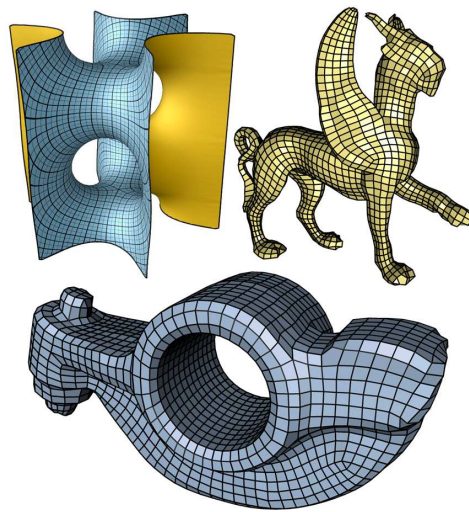
Automatically generated quadrilateral meshes from given irregular triangle meshes.

References

[1] F. Kälberer, M. Nieser, and K. Polthier, *QuadCover - Surface Parameterization using Branched Coverings*, submitted (2007).
[2] S. Dong, S. Kircher, and M. Garland. *Harmonic functions for quadrilateral remeshing of arbitrary manifolds*, Computer Aided Design, 22(4) (2005), 392–423.
[3] X. Gu and S.-T. Yau. *Global conformal surface parameterization*, Symp. on Geom. Proc. (2003), 127–137.
[4] L. Kharevych, B. Springborn, and P. Schröder. *Discrete conformal mappings via circle patterns*, ACM Trans. on Graph. 25(2) (2006).
[5] M. Marinov and L. Kobbelt. *A robust two-step procedure for quad-dominant remeshing*, Comp. Graphics Forum 25(3) (2006).
[6] N. Ray, W. C. Li, B. Lévy, A. Sheffer, and P. Alliez. *Periodic global parameterization*, ACM Trans. on Graph. 25(4) (2006), 1460–1485.
[7] Y. Tong, P. Alliez, D. Cohen-Steiner, and M. Desbrun. *Designing quadrangulations with discrete harmonic forms*, Symp. on Geom. Proc. (2006) 201–210.

Discrete Differential Geometry for Architecture

Helmut Pottmann

(joint work with A. Bobenko, Y. Liu, J. Wallner, W. Wang)

Freeform shapes in architecture is an area of great engineering challenges and novel design ideas. Obviously the design process, which involves shape, feasible segmentation into discrete parts, functionality, materials, statics and cost at every stage benefits from a complete knowledge of the complex interrelations between geometry requirements and available degrees of freedom. Only recently researchers have become interested in the geometric basics of single- and multi-layer architectural freeform structures based on polyhedral surfaces.

The talk reports on recent progress in this emerging field of research, which is situated at the meeting point of discrete differential geometry, modeling, geometry processing and architectural design. The mathematical topics include mesh

parallelism, discrete Gauss images, a discrete curvature theory and results on especially useful meshes such as discretizations of principal curvature lines, edge offset meshes and discrete surfaces with constant mean or Gaussian curvature. The results can be formulated within relative differential geometry and in this way provide additional flexibility for the desired applications.

REFERENCES

[1] Y.Liu, H. Pottmann, J. Wallner, Y. Yang, W. Wang, *Geometric modeling with conical meshes and developable surfaces*, ACM Trans. Graphics **25** (2006), 681–689.
[2] H. Pottmann, A. Bobenko, Y.Liu, J. Wallner, W. Wang, *Geometry of multi-layer freeform structures for architecture* , submitted for publication.

Analysis of Subdivision Surfaces near Extraordinary Vertices
Ulrich Reif

Due to their simple and efficient algorithmic structure, subdivision surfaces have become the standard primitive for the generation of smooth surfaces of arbitrary topological genus in computer graphics applications. By contrast, the mathematical analysis of the underlying algorithms is nontrivial and still poses some challenging questions.

Let us briefly review some basic principles for an analytic approach. The representation of subdivision surfaces as an infinite union of spline rings,

$$\mathbf{x} = \bigcup_{m \in \mathbb{N}_0} \mathbf{x}^m, \quad \mathbf{x}^m : \Omega \to \mathbb{R}^3, \quad \Omega := [0,2]^2 \backslash [0,1)^2 \times \{1, \ldots, n\},$$

is quite different from the algorithmic point of view, where they are considered as the limit of a sequence of finer and finer polygonal meshes. In the case of linear stationary subdivision, the spline rings are given by

$$\mathbf{x}^m = BA^m \mathbf{P},$$

where B is a column vector of basis functions, $\mathbf{P}$ is a column vector of control points, and A is the subdivision matrix. Using the eigen-decomposition $A = V\Lambda V^{-1}$, we define the eigenfunctions and -coefficients by $F := BV$ and $\mathbf{Q} := V^{-1}\mathbf{P}$, respectively, to obtain the expansion

$$\mathbf{x}^m = \sum_{\ell=0}^{L} \lambda^m f_\ell \mathbf{q}_\ell.$$

Convergence of the scheme is guaranteed if the dominant eigenvalue is $\lambda_0 = 1$. Schemes with a double subdominant eigenvalue $\lambda := \lambda_1 = \lambda_2$, generate C^1-surfaces if the characteristic map

$$\Psi := [f_1, f_2] : \Omega \to \mathbb{R}^2$$

is regular and injective. All schemes currently is use satisfy to this condition. However, subdivision surfaces do not live up to the high demands encountered, for instance, in industrial car body design. In order to understand the sources

of shape artifacts, the limit behavior of curvature has to be analyzed. Standard tools, like principal curvatures and directions are not suitable since in case of an umbillic limit point, the principal directions do not converge, even if the surface is perfectly smooth. The Weingarten map W, which relates the differential of the Gauss map and the parametrization via

$$-D\mathbf{n} = W D\mathbf{x}$$

is also not useful since its representation depends on the basis of the tangent space, which is typically given by the partial derivatives of $\mathbf{x}$, and these vectors are discontinuous for subdivision surfaces. We suggest to employ the *embedded Weingarten map* E, which is defined by

$$\begin{bmatrix} -D\mathbf{n} \\ 0 \end{bmatrix} = \begin{bmatrix} D\mathbf{x} \\ \mathbf{n} \end{bmatrix} E,$$

and can easily be computed with the help of the pseudo inverse $D\mathbf{x}^+$ of $D\mathbf{x}$ and the second fundamental form,

$$E = D\mathbf{x}^+ \, II \, (D\mathbf{x}^+)^{\mathrm{t}}.$$

Besides the trivial eigenvalue 0 corresponding to the normal direction, we have

$$\mathbf{r}_i E = \kappa_i \mathbf{r}_i, \quad i \in \{1, 2\},$$

where κ_i are the principal curvatures to the principal directions $\mathbf{r}_i$. Compared with the relatively complicated integrability conditions for the fundamental forms (Mainardi-Codazzi and Gauss), the integrability conditions for E simply read

$$\mathbf{n}_s E_t^+ = \mathbf{n}_t E_s^+.$$

Moreover, E is a geometric invariant of the surface, and is ideally suited for curvature analysis of subdivision surfaces. The asymptotic expansion of E^m is

$$E^m = (\mu/\lambda^2)^m \begin{bmatrix} E^c & 0 \\ 0 & 0 \end{bmatrix} + O(\mu)^2,$$

where $\mu := \lambda_3 = \cdots = \lambda_r$ is the subsub-dominant eigenvalue of A, and E^c can be easily computed from the characteristic map and the second fundamental form of the central surface

$$\tilde{\mathbf{x}} := f_1 \mathbf{q}_1 + f_2 \mathbf{q}_2 + \sum_{\ell=3}^{r} \langle \mathbf{q}_\ell, \mathbf{n} \rangle f_\ell.$$

A necessary and sufficient condition for a scheme to generate C^2-surfaces is $\mu = \lambda^2$, and that the limit matrix E^c is constant. The latter property is equivalent to

$$f_\ell \in \mathrm{span}\, \{f_1^2, f_1 f_2, f_2^2\}, \quad \ell = 3, \ldots, r.$$

A first algorithm satisfying this extremely restrictive functional condition was given in [4], but it did not become popular due to a severe lack of flexibility. Recently, Peters and Karciauskas [1] pioneered the idea of guided subdivision, which is the first instance of a C^2-algorithm combining ease of use and high surface quality. Inspired by their ideas, we propose a new framework for the construction of a broad class of C^2-schemes: Denote the space of C^2-spline rings of bi-degree d with

values in $\mathbb{R}^s$ by $C_d^2(\Omega, \mathbb{R}^s)$, and choose a *concentric tessellation map* $\Psi \in C_d^2(\Omega, \mathbb{R}^2)$, which is regular and injective, and joins C^2 with $\lambda \Psi$ for a given value $\lambda \in (0, 1)$. Then the scheme proceeds in four linear steps:

(1) *Reparametrization.* Given a spline ring $\mathbf{x} = B\mathbf{P} \in C_{2d}^2(\Omega, \mathbb{R}^3)$, let

$$\mathbf{r} := R[\mathbf{x}] = \mathbf{x} \circ \Psi^{-1}$$

denote the reparametrization of $\mathbf{x}$ over the set $\Gamma := \mathbf{x}(\Omega)$.

(2) *Extension.* Define an extension

$$\mathbf{e} := E[\mathbf{r}], \quad \mathbf{e} : \lambda\Gamma \to \mathbb{R}^s$$

of $\mathbf{r}$ with the property that $\mathbf{r}$ and $\mathbf{e}$ join C^2 and that $\mathbf{r} \in \mathbb{P}_d$ implies $\mathbf{e} \in \mathbb{P}_d$, where $\mathbb{P}_d$ denotes the space of all bivariate polynomials of total degree d. For instance, extension operators can be derived from minimizing standard fourth order fairness functionals.

(3) *Turn back.* The function $\mathbf{r}_e$ is turned back to a spline ring by

$$\mathbf{t} := T[\mathbf{e}] = \mathbf{e} \circ \Psi.$$

(4) *Projection.* Finally, the spline ring $\mathbf{t}$ is projected onto the given spline space,

$$\mathbf{p} := P[\mathbf{t}] \in C_{2d}^2(\Omega, \mathbb{R}^3),$$

for instance by minimizing a standard distance functional.

Together, we obtain the subdivision scheme

$$S[\mathbf{x}] := P[T[E[R[\mathbf{x}]]]].$$

By construction, the corresponding subdivision matrix A has eigenvalues

$$1, \lambda, \lambda, \lambda^2, \lambda^2, \lambda^2,$$

and it defines a C^2 scheme if and only if all remaining eigenvalues are less than λ^2 in modulus. The minimal possible value of d is $d = 3$ so that the spline rings have to be at least bi-sextic.

REFERENCES

[1] K. Karciauskas and J. Peters, *Concentric Tessellation Maps and Curvature Continuous Guided Surfaces*, to appear in CAGD, (2007).
[2] J. Peters and . Reif, *Shape characterization of subdivision surfaces-basic principles*, CAGD, **21** (2004), 585-599.
[3] U. Reif and J. Peters, *Structural Analysis of Subdivision Surfaces – A Summary*, in Topics in Multivariate Approximation and interpolation, K. Jetter et al. (eds.), Elsevier, (2006), 149-190.
[4] U. Reif, *TURBS – Topologically Unrestricted Rational B-Splines*, Constructive Approximation, **14** (1998), (47-77).

Adaptive Markov Models with Information-Theoretic Methods for Image Analysis

Ross Whitaker

(joint work with Suyash Awate, Tolga Tasdizen)

1. Introduction

Low-level problems in image processing, such as denoising, reconstruction, and segmentation typically require some kind of model of image structure. Thus, the modeling of images in a general, yet tractable manner remains an important area of research. Most image processing algorithms make strong geometric or statistical assumptions about the properties of the signal and/or noise. Therefore, they lack the generality to be easily applied to new applications or diverse image collections. This talk presents an adaptive Markov model of images that allows algorithms to automatically learn the local statistical dependencies of image neighborhoods. Probability densities for neighborhoods are estimated nonparametrically, through a kernel-based strategy, and thus, image statistics are captured through large sets of examples of image neighborhoods. We use this strategy to create adaptive algorithms for low-level image processing. We enforce optimality criteria based on fundamental information-theoretic concepts that capture the functional dependence, information content, and uncertainty in the data. This talk presents examples of the application of this strategy to denoising, reconstruction, and segmentation.

2. Random-Field Image Model

The proposed methodology develops from the model of an image as a random field. A random field [12] is a family of random variables $X(\Omega; T)$, for some index set T, where, for each fixed $T = t$, the random variable $X(\Omega; t)$ is defined on the sample space Ω. If we let T be a set of points defined on a discrete Cartesian grid and fix $\Omega = \omega$, we have a realization of the random field called the *digital image*, $X(\omega, T)$. In this case $\{t\}_{t \in T}$ is the set of pixels in the image. For two-dimensional images t is a two-vector. If we fix $T = t$ and let ω vary then $X(t)$ is a random variable on the sample space. We denote a specific realization $X(\omega; t)$ (the intensity at pixel t), as a deterministic function $x(t)$.

If we associate with T a family of pixel neighborhoods $N = \{N_t\}_{t \in T}$ such that $N_t \subset T$, $t \notin N_t$, and $u \in N_t$ if and only if $t \in N_u$, then N is called a neighborhood system for the set T. Points in N_t are called neighbors of t. We define a random vector $Y(t) = \{X(t)\}_{t \in N_t}$ corresponding to the set of intensities at the neighbors of pixel t. We also define a random vector $Z(t) = (X(t), Y(t))$ to denote image regions, i.e. pixels combined with their neighborhoods. The proposed formulation assumes a stationary ergodic process (in practice this assumption can be relaxed somewhat)

3. Processing With Density Functions

The proposed strategy is to model the probability density functions associated with the neighborhood, which are the joint distribution $P(z)$ and the conditional distribution $P(\tilde{x}|\tilde{y})$, and use these models to either denoise or classify pixels in images.

For denoising, we propose an *entropy scale-space* that is a gradient descent of the joint entropy

$$h(Z) = -\sum_{t \in T} \log P\left(Z(t)\right) dt$$

where T is the image domain.

The probabilities associated with these neighborhoods are formed from image examples—that is, set of randomly selected neighborhoods from around the image—and a kernel-based estimation, also called Parzen windowing. Thus, we have

$$P(Z = z_i) \approx \frac{1}{|A_i|} \sum_{t_j \in A_i} G_n(z_i - z_j, \sigma)$$

where G_n is an isotropic Gaussian kernel with standard deviation σ. For the entropy this gives

$$h(Z) = -\sum_i \log \left(\frac{1}{|A_i|} \sum_{t_j \in A_i} G_n(z_i - z_j, \sigma) \right),$$

where z_i is the neighborhood at the i pixel location, and A_i is a set of image samples choose to model the density for that point.

The proposed algorithm uses a gradient descent of the joint entropy with respect to x_i. We express the update descent in terms of a dummy evolution parameter, τ, which gives

$$\frac{\partial x_i}{\partial \tau} = -\frac{\partial h(Z)}{\partial x_i} \approx -\frac{1}{|T|\sigma^2} \sum_{t_j \in A_i} \frac{G_n(z_i - z_j, \Psi_n)}{\sum_{t_k \in A_i} G_n(z_i - z_k, \Psi_n)} (x_i - x_j)$$

If we choose discrete updates with a time step $|T|\sigma^2$, then we have the following iterative procedure for each pixel

$$x_i^{n+1} \longleftarrow \sum_j w_{i,j} x_j$$

where the sum over j covers the random selection of samples and $w_{i,j}$s are formed by Gaussian kernels and $\sum_j w_{i,j} = 1$. Thus, each pixel update is formed by a weighted some of other pixel values whose neighborhoods are similar to the pixel being updated. We call this algorithm *UINTA* [11, 2]. Replacing pixel values with weighted averages of pixels with similar neighborhoods has also been proposed [8, 7], in the algorithm *NL-means*, which performs only one update with a fairly large averaging window. This analysis shows that NL-means a special case, a single iteration, of the iterative, entropy reducing procedure defined by UINTA.

An important practical aspect of the algorithm is the selection of σ. For this application we propose σ that maximizes the likelihood of each sample, using a cross validation strategy—which also minimizes entropy. Thus *sigma* is driven by the information content of the image, and is updated each iteration, as the randomness in the image is reduced.

More details on this method and extensive experimental results are presented in a series of papers [11, 2, 13]. These results show that the algorithm is quite effective compared to state-of-the-art methods based on PDEs and wavelet shrinkage. These results also show that iterative approach with an automatic selection of σ generally outperforms the *one-shot* strategy of NL-means, which requires a much larger σ in order to be effective at all.

4. Other Applications

The proposed strategy, of modeling probability densities of image neighborhoods with sets of neighborhoods samples has other applications. For instance, if we include a noise model, or likelihood, we can use the joint neighborhood density as a prior, and perform an optimal, a-posteriori estimation that properly weights the input data and the neighborhood densities. This has been shown to be effective, for instance, in denoising MRI data of the human head [5].

This strategy also has applications in image segmentation. For instance, in MRI tissue classification, the intensities of MRI images are generally not sufficient to make reliable decisions about tissue type, especially at the interface between different tissue types. Thus, several authors propose the use of Markov random fields, to explicitly bias solutions toward smoother tissue boundaries. Nonparametric neighborhood models, combined with an entropy reduction scheme for each tissue type, have been shown to be more effective for reducing classification error [4, 1]. The strategy of reducing in-class neighborhood entropy is also effective for texture classification [3].

References

[1] S. Awate, T. Tasdizen, R. Whitaker, N. Foster, *Adaptive, Nonparametric Markov Modeling for Unsupervised, MRI Brain-Tissue Classification*, Medical Image Analysis (2006).

[2] S. Awate, R. Whitaker, *Unsupervised, Information-Theoretic, Adaptive Image Filtering for Image Restoration*, IEEE Trans. on Pattern Analysis and Machine Intelligence, **28(3)** (2005), 364–376.

[3] S. Awate, T. Tasdizen, R. Whitaker, *Unsupervised Texture Segmentation with Nonparametric Neighborhood Statistics*, European Conference on Computer Vision (ECCV 2005), 494–507.

[4] T. Tasdizen, S. Awate, R. Whitaker, N. Foster, *MRI Tissue Classification with Neighborhood Statistics: A Nonparametric, Entropy-Minimizing Approach'*, Medical Imaging Computing and Computer-Assisted Intervention (MICCAI 2005), 517–525.

[5] S. Awate, R. Whitaker, *Nonparametric Neighborhood Statistics for MRI Denoising* Information Processing in Medical Imaging (IPMI 2005), 677–688.

[6]

[7] A. Buades, B. Coll, J.M Morel, *A review of image denoising algorithms, with a new one*, SIAM Multiscale Modeling and Simulation **4(2)** (2005), 490–530.

[8] A. Buades, B. Coll, J.-M. Morel *A non local algorithm for image denoising*, IEEE Int. Conf. on Computer Vision and Pattern Recognition (CVPR 2005), 60–65.

[9] Leemput, K.V., Maes, F., Vandermeulen, D., Seutens, P.: *Automated model-based tissue classification of mr images of the brain*, IEEE Tr. Med. Imaging **18** (1999) 897–908

[10] Kapur, T., Grimson, W.E.L., Wells, W.M., Kikinis, R., *Segmentation of brain tissue from magentic resonance images*, Med. Im. An. **1** (1996), 109–127.

[11] S. Awate, R. Whitaker, *Image Denoising with Unsupervised Information-Theoretic Adaptive Filtering*, International Conference on Computer Vision and Pattern Recognition (CVPR 2005), 44–51.

[12] Dougherty, E.R., *Random Processes for Image and Signal Processing*, Wiley (1998).

[13] S. Awate, *Adaptive, Nonparametric Markov Models and Information-Theoretic Methods for Image Restoration and Segmentation*, Univeristy of Utah Ph.D. Dissertation, (2006).

Reporters: Bernhard Mößner, Martina Teusner